Highlights

Continuous decentralized hydrogen production through alkaline water electrolysis powered by an oxygen-enriched air integrated biomass gasification combined cycle

Roque Aguado, Andrea Baccioli, Angelica Liponi, David Vera

- A novel approach for decentralized green hydrogen production from biomass is explored.
- An integrated gasification combined cycle is hybridized with an alkaline electrolyzer.
- The oxygen by-product from the electrolyzer is mixed with air to fire a downdraft gasifier.
- An upgraded producer gas with a lower heating value of 7–8 MJ/Nm^3 can be obtained.
- A global efficiency of 17.6% based on the lower heating value of hydrogen can be reached.

Continuous decentralized hydrogen production through alkaline water electrolysis powered by an oxygen-enriched air integrated biomass gasification combined cycle

Roque Aguado[a,*], Andrea Baccioli[b], Angelica Liponi[b], David Vera[a]

[a]*Departamento de Ingeniería Eléctrica, Escuela Politécnica Superior de Linares, Universidad de Jaén, Avda. de la Universidad s/n, 23700, Linares, Spain*
[b]*Dipartimento di Ingegneria dell'Energia, dei Sistemi, del Territorio e delle Costruzioni, Università di Pisa, Largo Lucio Lazzarino, 56122, Pisa, Italy*

Abstract

This research work presents an innovative approach for continuous decentralized production of renewable hydrogen from woody biomass. Alkaline water electrolysis (AWE) is used to produce high-purity hydrogen, while the oxygen by-product is mixed with ambient air and used to fire a biomass-fueled downdraft gasifier in order to produce an upgraded producer gas with a lower heating value (LHV) between 7–8 MJ/Nm^3. This fuel gas is then subjected to a conditioning stage and eventually fed to a combined cycle consisting of a recuperative gas turbine as topping unit and a regenerative subcritical organic Rankine cycle as bottoming unit, which together allow for a combined electric power generation efficiency close to 40%. Most of the net AC power from the integrated gasification combined cycle (IGCC) is rectified to DC power and ultimately used to power an alkaline electrolyzer, with a minor share allocated to all the required utilities and ancillary equipment, including hydrogen compression to 200 bar. The results from simulation of the hybrid IGCC-AWE plant under steady-state operating conditions in Aspen Plus V.11 indicate an optimal efficiency of 17.6% based on the LHV of hydrogen. Thus, if sized for a biomass consumption of 1 t/h, the proposed plant is capable of providing around 26 kg/h of compressed hydrogen at 200 bar.

Keywords: Green hydrogen, Producer gas, Downdraft gasifier, Gas turbine, Organic Rankine cycle, Alkaline water electrolyzer

1. Introduction

Climate change and fossil fuel depletion are the main drivers for the current energy transition efforts toward a decarbonized economy. Among the ongoing initiatives to keep global warming

*Corresponding author
Email addresses: ramolina@ujaen.es (Roque Aguado), andrea.baccioli@unipi.it (Andrea Baccioli), angelica.liponi@phd.unipi.it (Angelica Liponi), dvera@ujaen.es (David Vera)

below 2 °C with respect to pre-industrial levels, a great deal of research is being conducted on hydrogen as an alternative energy vector to fossil fuels [1]. Nowadays, the overwhelming majority of the world's hydrogen production (~96%) still comes from fossil resources [2, 3], at unbeatable costs if the CO_2 emissions are not captured and sequestered, in which case the hydrogen produced is conventionally termed "gray hydrogen" [4]. The main sources of hydrogen production are the processes of steam reforming of light hydrocarbons and partial oxidation of heavier hydrocarbons, which together account for 78% of the global hydrogen production, while coal gasification is responsible for the remaining 18% [5, 6]. Alternatively, hydrogen can be sustainably produced from renewable energy sources, which constitutes the so-called "green hydrogen" [4–6]. Renewable hydrogen production is quickly approaching economic competitiveness and enjoying unprecedented political and business momentum, with the number of favorable policies and projects worldwide expected to increase rapidly in the coming years [4]. Among these alternative hydrogen production pathways, water splitting through the process of electrolysis exhibits the highest technology readiness level at TRL 9 [2]. In fact, the process of water electrolysis currently supplies most of the remaining 4% of the global hydrogen production, with negligible amounts of hydrogen from other hydrogen production technologies on an industrial scale [7, 8]. Thus, the combination of water electrolysis and renewable energy for sustainable hydrogen production is often regarded as an essential step toward decarbonization of industrial processes and the transport sector [8].

Alkaline water electrolysis (AWE) currently represents the most economical and mature technology for electrolytic hydrogen production, standing out from other water electrolysis technologies in terms of cost and simplicity [7, 9–12]. In fact, alkaline electrolyzers have been on the market for many decades and are by far the most widely used [7, 9]. In addition, they have already been demonstrated in large-scale hydrogen production plants [10, 12, 13]. The electrolyte used in conventional alkaline water electrolyzers has traditionally been 20–35% by weight aqueous potassium hydroxide (KOH) solutions [10, 13, 14], because of the optimal conductivity and remarkable corrosion resistance of stainless steel in this concentration range [14]. The operating temperature

ranges between 60–90 °C and the pressure is usually below 30–50 bar in most cases [10, 13, 15], although some systems can reach up to 200 bar [16]. State-of-the-art alkaline electrolyzers are reliable, have energy efficiencies of 50–70%, and operate at cell voltages of 1.7–2.4 V and current densities below 0.5 A/cm^2 [5, 7, 13]. Moreover, they operate with few moving parts, require little space and maintenance costs are low [17]. Actually, electrolyzers show an availability of at least 98% and balance of plant (BOP) equipment is sufficiently mature that it is not necessary to save a certain shut-down time for maintenance [18]. The purity of the hydrogen directly produced from alkaline water electrolysis may be greater than 99.5% [5, 7, 8, 10, 13, 19, 20], and only drying and compression are required to arrive at normal merchant quality [21]. Another advantage of alkaline electrolyzers over other types lies in the durability of their components, which allows a much longer lifetime, ranging from 20 to 30 years [5, 7, 16]. However, they suffer from a few major limitations that must be considered when operating with fluctuating renewable energy sources such as solar and wind power [11]. Specifically, conventional alkaline electrolyzers are designed for operation at fixed process conditions [8]. Consequently, partial load operation of alkaline electrolyzers is restricted to the range of 20–100% of their nominal electric power [7, 9, 11, 13, 15], which poses a challenge for dynamic operation in an electricity grid dominated by fluctuating power generation [12]. Indeed, there is a significant risk of the formation of potentially flammable mixtures of hydrogen and oxygen, due to diffusion of both gases through the electrolyzer membranes when the operating current is excessively low [8, 11, 13]. Furthermore, the number of start-ups and stops must be limited to avoid a significant reduction of the electrolyzer lifetime [11], due to the corrosive nature of the electrolyte [12]. In order to overcome all these limitations, the use of dispatchable renewable energy sources such as biomass resources can significantly support or even displace the non-continuous electrolytic production of green hydrogen coming from intermittent and unpredictable renewable energy sources [1]. Moreover, the use of biomass resources as controllable renewable energy sources can effectively result in hydrogen cost reductions by increasing the utilization factor of alkaline electrolyzers. In this regard, it is worth noting that direct produc-

tion of hydrogen from fluctuating renewable energy sources such as solar or wind power is not the best solution from an economic standpoint because of the low utilization factor of the electrolyzer [22].

In the water electrolysis process, a volume of oxygen equal to half the volume of electrolytic hydrogen is simultaneously generated as a by-product [23]. Thus, if large amounts of electrolytic hydrogen are to be produced from renewable energy resources, oxygen will also be by-produced on a large scale [23]. However, in the overwhelming majority of the research and industrial processes that use electrolysis to produce hydrogen, oxygen is usually vented into the atmosphere as a worthless by-product [9, 20]. In light of this fact, another key advantage of using biomass as renewable energy source is that the oxygen by-product from the water electrolysis process can be used on-site as oxidizing agent instead of ambient air. Indeed, the electrolytic oxygen has already been explored in oxy-fuel hybrid systems for long-term energy storage through the production of synthetic natural gas (SNG) or methanol using surplus power from intermittent renewable sources, following an approach known as "power to gas" (PtG) or "power to liquid" (PtL), respectively [20, 24–29]. In order to make the most of the by-produced oxygen, biomass equipment can be operated well below the stoichiometric oxygen requirement so that gasification, rather than combustion, occurs [26]. Gasification is a thermochemical conversion process, whereby a carbonaceous solid feedstock such as biomass is partially oxidized by a gasifying agent and converted into a gaseous fuel [30]. Ambient air is often the preferred choice as gasifying agent for economic reasons, but in such cases, a substantial amount of nitrogen is present in the gas mixture as well, which leads to a highly diluted gaseous fuel with low calorific value (LHV = 4–6 MJ/Nm^3), the term used for which is producer gas [30]. In the particular case of air-blown biomass gasification, the producer gas is composed of carbon monoxide (CO), hydrogen (H_2), carbon dioxide (CO_2), methane (CH_4), water vapor (H_2O) and nitrogen (N_2), in addition to smaller fractions of other light hydrocarbons that are typically in gaseous state at ambient conditions (mostly, C_2 to C_4) and trace amounts of various contaminants such as tar, ash, and soot [3, 29–31]. However, using the already available

oxygen from water electrolysis instead of ambient air as gasifying agent can avoid or significantly reduce nitrogen dilution, thereby leading to an upgraded producer gas with higher energy density. Oxygen-blown gasification can generate a gaseous product with high calorific value gas (LHV = 10–15 MJ/Nm^3) known as synthesis gas or syngas [30], but the oxygen production cost is usually excessively expensive for industrial utilization [32]. The use of oxygen-enriched air is therefore of great interest if an upgraded producer gas with medium to high calorific values can be generated at a reasonable cost [32]. The upgraded producer gas from oxygen-enriched air biomass gasification, once conditioned to remove the aforementioned contaminants, can be fueled to internal combustion engines, internally fired gas turbines or even fuel cells for power generation.

Hydrogen production from biomass gasification can contribute to reducing the net emissions of greenhouse gases into the atmosphere, since biomass resources are regarded as a carbon-neutral feedstock due to their short life cycle [33]. Instead of water splitting through the process of electrolysis, another approach to producing renewable hydrogen from biomass gasification is to concentrate and separate the hydrogen content in the producer gas, but this hydrogen production approach has not yet been tested on a demonstration scale near the desired configuration in terms of performance, weight, and volume [2, 21]. Hydrogen production from producer gas or syngas requires several complex downstream processing operations, which typically involve increasing the yield of hydrogen through the water gas shift reaction through the use of catalyzed reactors [3, 34], which are sensitive units to coking, catalyst poisoning, tar deposition etc. [3], in addition to partial separation of the resulting hydrogen from other gaseous components in a pressure swing adsorption (PSA) unit or through membrane processes [35]. The pressurized equipment for downstream processing of the producer gas also requires additional power consumption for compression [35, 36], while steam generation represents another important energy consumption. Furthermore, for the purpose of high-purity hydrogen production, it is necessary to produce a nitrogen-free gas, so air gasification processes are usually disregarded [21], and thus, the gasifier must be fired with an external source of oxygen, which significantly adds to the cost of the system [1]. However, since

the oxygen by-product from water electrolysis is typically underutilized, it can be used to enrich ambient air as gasifying agent, thereby increasing the efficiency of the combined system [23]. Accordingly, a hybrid system consisting of an alkaline electrolyzer and a biomass gasification plant is proposed and simulated in this work for continuous decentralized hydrogen production. The power generation unit considered is a combined cycle power plant fueled with upgraded producer gas consisting of a gas turbine topping cycle and a subcritical organic Rankine bottoming cycle, similarly to a conventional integrated gasification combined cycle (IGCC) plant, but adapted to small-scale power generation and hybridized with alkaline water electrolysis. In this regard, it is worth noting that unlike large-scale IGCC plants, which conventionally include a heat recovery steam generator (HRSG) to drive a steam Rankine bottoming cycle, very few works are available on IGCC plants with low-temperature bottoming cycles for small-scale power generation [37, 38]. Moreover, even though biomass-fueled IGCC systems based on two-stage oxygen-enriched air gasification have recently been proposed for clean and efficient biomass utilization [39], it is not known of previous work aimed at hybridization of IGCC plants and alkaline water electrolyzers for hydrogen production. Biomass-fueled IGCC plants have already been shown to have the potential to contribute to reducing the environmental impact of power generation [40]. Thus, the use of biomass resources as feedstock to the hybrid IGCC-AWE plant can provide an alternative renewable solution for decarbonization of industrial sectors that often require a stable supply of hydrogen, such as in the food processing, iron and steel making or ammonia production industries [2, 4, 35].

2. Plant description and process modeling

A schematic process flow diagram of the hybrid IGCC-AWE plant for continuous decentralized hydrogen production from biomass is presented in Fig. 1. The proposed plant incorporates an alkaline water electrolyzer, the main advantages of which are its much higher technological maturity, cost-competitiveness, and durability as compared to other available electrolytic hydro-

gen production alternatives [9–12, 20]. The hydrogen output is compressed and stored for further use, while the oxygen by-product is mixed with ambient air to fire a biomass-fueled downdraft gasifier, thereby reducing nitrogen dilution of the producer gas. Thereafter, a producer gas conditioning unit consisting of a cyclone, a wet scrubber, and several filters is included downstream of the gasifier. The clean upgraded producer gas is eventually fueled to a gas turbine in order to generate power in a recuperative Brayton cycle. Waste heat from the exhaust gas cooling process is recovered through an organic Rankine cycle (ORC) bottoming unit to generate additional power. The combined system is capable of delivering the stable renewable power required by the alkaline electrolyzer for hydrogen production, while the oxygen by-product is efficiently utilized to partially oxidize the biomass feedstock. A major advantage of this configuration is that all the different units are proven in operational environments, commercially available, and can be modular. Thus, the IGCC plant is rather flexible and, in case no hydrogen production is required, it can be fired with ambient air and be operated to solely provide stable electric power. In addition to the power required by the electrolyzer, the power consumption by the utilities and BOP equipment is supplied by the own power generation in the IGCC plant, and hence, off-grid operation is possible. However, grid connection would be advantageous during plant commissioning and start-up.

The hybrid IGCC-AWE plant for continuous decentralized hydrogen production from biomass was simulated under steady-state operating conditions using the commercial software Aspen Plus V.11 by Aspen Technology Inc. (AspenTech). Aspen Plus was the preferred choice over other process simulators because of its large degree of flexibility in handling solids and non-conventional materials, as well as the option to insert customized statements in Fortran code. Non-conventional components include solid materials of heterogeneous nature such as biomass and ash, which cannot be precisely characterized by their chemical formulas [41, 42]. MCINCPSD stream class comprising three substreams of MIXED, CIPSD and NCPSD is used to define the structure of biomass and ash streams, which are not available in the Aspen Plus component database. The lower heating value, formation enthalpy, and density of these non-conventional components are estimated from

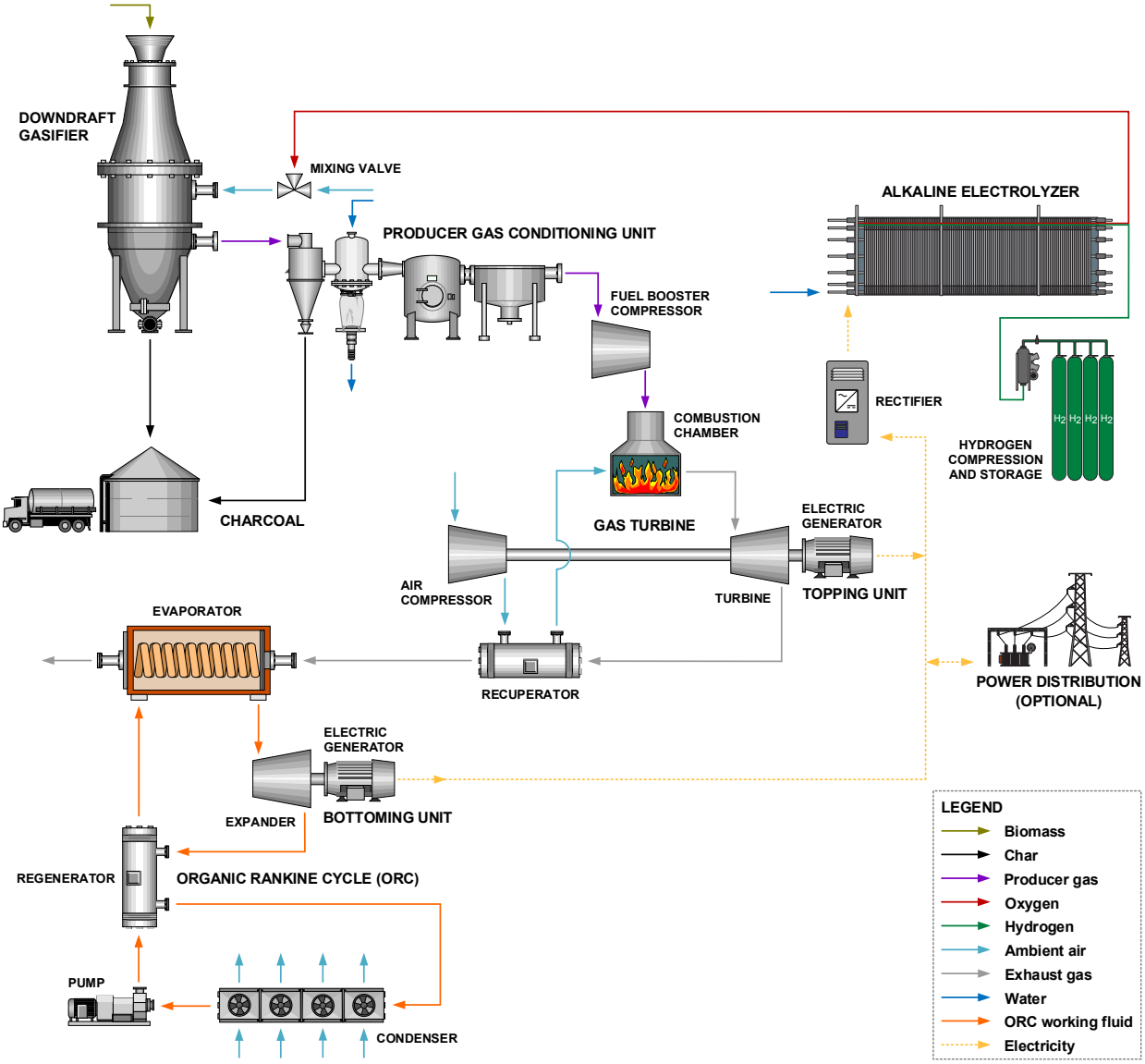

Figure 1: Design process flow diagram of the hybrid IGCC-AWE plant for continuous decentralized hydrogen production from biomass.

their proximate and ultimate analyses by means of the HCOALGEN and DCOALIGT models [19, 35, 41–45]. Both models were originally developed for coal, but are experimentally validated for biomass materials with a reasonably good approximation. The HCOALGEN model includes different empirical correlations to estimate heat of combustion, enthalpy of formation, and specific heat; whereas the DCOALIGT model is based on empirical correlations from the Institute of Gas Technology (IGT) to estimate density [44]. The heat of combustion in the HCOALGEN model is

a gross calorific value on a dry ash-free basis, which is automatically estimated through the empirical correlation of Boie [46]. The Peng–Robinson cubic equation of state with Boston–Mathias alpha function (PR-BM) is used to estimate the thermodynamic properties of all the conventional components [44], which is appropriate for gasification processes where the temperature is quite high [47]. The following assumptions were made for the simulation of the hybrid IGCC-AWE plant in Aspen Plus:

- Generic woody biomass pellets are considered as input feedstock to the hybrid IGCC-AWE plant [26, 33, 38, 40, 44, 48]. The biomass feedstock is assumed to have an ultimate analysis of 51.3% C, 6.3% H, 42.0% O, 0.1% N, and 0.3% ash [49]; in addition to a moisture content of 6% (wet basis) [47, 49], and a lower heating value (LHV) of 19.18 MJ/kg (dry ash-free basis) [49]. However, it should be noted that the IGCC-AWE hybrid plant can be fed with any lignocellulosic biomass source that meets the requirements for use in fixed-bed gasifiers. In particular, the biomass feedstock should have a moisture content below 15% (wet basis), a low ash content (preferably below 5%) and a suitable particle size, which should remain in the range of 3–51 mm [30].
- The plant is operating under steady-state conditions within a zero-dimensional and time-independent approach where hydrodynamic effects are neglected.
- All chemical reactions reach thermodynamic equilibrium conditions and reaction kinetics are not considered. Perfect mixing and uniform temperature and pressure profiles are assumed inside chemical reactors.
- Environment and reference state definition according to the IUPAC Standard Ambient Temperature and Pressure (SATP) conditions of T_a = 25 °C and P_a = 1 bar.
- The ambient air is at SATP conditions, with the following molar composition: 20.75% O_2, 77.29% N_2, 0.92% Ar, 0.03% CO_2 and 1.01% H_2O.

Fig. 2 displays the process flowsheet of the hybrid IGCC-AWE plant for renewable hydrogen production from biomass in the Aspen Plus simulation environment. Five different subsystems can

be identified: biomass gasification, producer gas conditioning, topping power cycle, bottoming power cycle, and alkaline water electrolysis. The detailed features of each of these subsystems are described hereinafter, along with their corresponding modeling approaches.

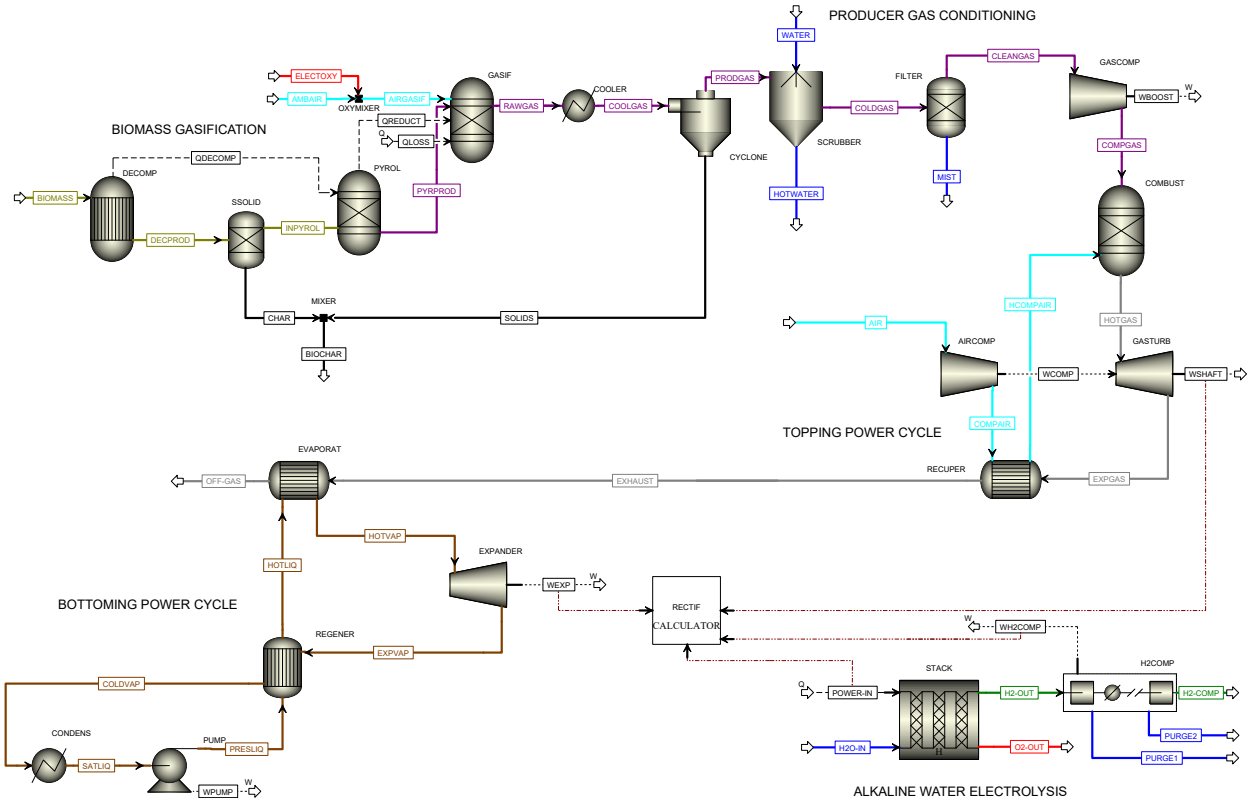

Figure 2: Process simulation flowsheet of the hybrid IGCC-AWE plant for continuous hydrogen production from biomass in Aspen Plus.

2.1. Biomass gasification

A downdraft fixed bed design is considered for the gasifier. This reactor configuration is characterized by the fact that the moving bed of biomass feedstock is directed together with the gasifying agent in the downward direction. As the biomass feedstock moves down toward the bottom of the gasifier, it undergoes several thermochemical reactions, which determine four different zones inside the gasifier, namely drying, pyrolysis, oxidation and reduction [30]. The choice of a downdraft fixed bed gasifier over other possible designs is due to several reasons. First of all, compared to fluidized bed and entrained flow gasifiers, fixed bed gasifiers are rather simpler reactors, but yet

also reliable [31], and most importantly, they involve a considerably lower capital investment and operational cost. Furthermore, it is possible to produce a gaseous fuel of similarly high quality (high concentration of carbon monoxide and hydrogen, low concentration of methane, heavier hydrocarbons and soot) and gasification efficiency during fixed bed gasification as during entrained flow gasification [49]. Another great advantage of downdraft gasifiers over most other designs is their comparatively lower tar production rate [30, 31], which allows a simpler and less robust producer gas conditioning unit with lower energy consumption [30]. Since nitrogen causes the reduction of the producer gas calorific value in air-blown gasification, using pure electrolytic oxygen as gasifying agent can avoid the dilution effect of nitrogen. However, in practice, the oxygen supply is often limited and using pure oxygen may not be cost-effective [32, 50]. Therefore, using oxygen-enriched air gas with electrolytic oxygen is a more desirable trade-off approach, since it can reduce the costs of commercial operation while improving the quality of the producer gas [50]. Accordingly, the downdraft gasifier is fired with a mixture of ambient air and electrolytic oxygen as gasifying agent and is operated at ambient pressure under autothermal conditions. Thereby, the biomass feedstock is partially oxidized by the oxygen-enriched air, producing enough heat to sustain the high-temperature atmosphere required for the producer gas formation. The main assumptions and simplifications in the biomass gasification process simulation are listed below:

- A modified non-stoichiometric equilibrium model based on minimization of Gibbs free energy was developed to predict the yield and composition of the producer gas. Thermodynamic equilibrium approaches have been widely adopted in the scientific literature for modeling downdraft gasifiers due to their low computational intensity and reasonable accuracy [32, 48]. In practice, the residence time of the reactants inside the gasifier is typically not long enough to attain a complete thermodynamic equilibrium. However, downdraft gasifiers are regarded to usually operate very close to equilibrium conditions [47, 51], especially at temperatures above 800 °C [52, 53], as a result of the faster reaction kinetics with increasing temperature and the sufficiently long residence time. Despite the downdraft

gasifier is intended to operate at high temperatures in conditions very close to thermodynamic equilibrium, a modified non-stoichiometric equilibrium approach is used, so that the small deviations with respect to the use of a purely non-stoichiometric equilibrium model are corrected with a good approximation [41, 54–56].

- Under thermodynamic equilibrium conditions at temperatures above 800 °C, the concentration of methane in the producer gas is negligible [32, 41]. In practice, however, the producer gas does not achieve complete equilibrium composition in downdraft gasifiers [41], as indicated by the presence of a significant content of methane [32, 47, 55]. Accordingly, the thermodynamic equilibrium model was slightly modified to avoid the underestimation of non-equilibrium products such as methane [54]. For this purpose, to prevent the complete consumption of methane in the gasification stage, a fraction of the methane formed during the pyrolysis process is by-passed to the gasifier outlet [41, 54–56]. As a result, the producer gas primarily contains hydrogen, carbon monoxide, carbon dioxide, water vapor and nitrogen along with methane, while the formation of heavier hydrocarbons is neglected [33].
- Tar formation was disregarded in order to reduce the complexity of the biomass gasification model [32, 42]. Since tar is not an equilibrium product, tar yield estimation in downdraft gasifiers is a challenge through a thermodynamic equilibrium modeling approach. As a result, tar is frequently either not included in thermodynamic equilibrium calculations or modeled as an inert compound (i.e., benzene, phenol and/or naphthalene) throughout the gasification process using empirical relations, where tar cracking and tar reduction reactions are not considered [57]. However, neglecting tar formation does not introduce significant deviations from reality, since downdraft gasifiers are recognized for their very low tar production [42], especially at higher operating temperatures. Moreover, the use of oxygen-enriched air as gasifying agent is more favorable for tar cracking, thereby improving the producer gas quality [43, 45, 50].
- A high operating temperature ($>$ 800 °C) in the gasifier is recommended to minimize the

tar content [41]. In fact, tar concentration is mainly a function of gasification temperature, decreasing as temperature increases [31, 43]. Due to the high temperatures reached in downdraft reactors (typically above 1000 °C), the tars formed in the pyrolysis zone are thermally cracked and burned immediately after in the oxidation zone in a phenomenon called flaming pyrolysis [30, 31, 56]. Thus, in order to make sure that tar destruction becomes almost complete, the oxygen supply was adjusted to keep the operating temperature in the downdraft gasifier above 1000 °C [49, 56].

- The carbon conversion efficiency is estimated at 95%, which is based on the average value from the experimental campaigns of an oxygen-blown downdraft gasifier fueled with wood pellets [49]. Therefore, it is assumed that 5% of the carbon content in the biomass feedstock remains unconverted and gets removed from the bottom of the gasifier together with ash [52, 54, 58]. As a result, the carbonaceous residue discharged from the gasifier (char) is only made up of carbon and ash [42, 43]. Ash is assumed as inert without catalytic activity and does not participate in the gasification process [32].
- About 7% of the total heat produced in the gasification process is released to the environment as radiation and convection heat losses from the surfaces of the gasifier [49, 56]. The relative heat losses are based on the chemical energy flow of the biomass feedstock [48, 56].

The pelletized and dried woody biomass feedstock (6% moisture content, wet basis) specified as a non-conventional component is introduced into the downdraft gasifier along with electrolytic oxygen. There is no in-built block available in Aspen Plus to represent a gasifier; and hence, a combination of several blocks is required to model the gasification process [41]. As mentioned above, downdraft gasifiers comprise four reaction zones, which do not correspond to any of the individual blocks shown in Fig. 2, but rather they are modeled together as a whole in a group of blocks. The biomass feedstock must initially be placed into a non-stoichiometric yield reactor (RYield), where the solid biomass is decomposed into its constituent elements by specifying the yield distribution according to its ultimate analysis [42, 43, 45, 47, 59, 60], due to the inability of

equilibrium reactors to directly calculate the yield distribution from non-conventional components such as biomass [42]. Biomass decomposition into its constituent elements is performed by calling an external Fortran subroutine. Char formation is modeled in another separator by removing a small fraction (5%) of carbon together with ash [47, 55, 56]. The remaining decomposed biomass feedstock then converts into hydrocarbons in a multiphase equilibrium reactor based on Gibbs free energy minimization (RGibbs) [60]. The partial oxidation and reduction reactions responsible for the producer gas formation are modeled together in another multiphase equilibrium reactor based on Gibbs free energy minimization [42, 43, 47, 48], where oxygen-enriched air is introduced as gasifying agent, along with the yield distribution of the devolatilized biomass feedstock. The yield of methane from the first multiphase equilibrium reactor is treated as a non-reacting feed component that does not participate in the thermodynamic equilibrium calculations of the second equilibrium reactor, where the oxidation and reduction zones are modeled together [54–56]. In other words, the yield of methane from biomass devolatilization is by-passed to the gasifier outlet to avoid underestimation of this component in the producer gas composition [60]. The heat of reaction originated during this last stage is transferred to the previous stages by means of heat streams to counterbalance the differences in enthalpy [42]. Heat losses to the surrounding environment are modeled through another user-programmed external Fortran statement [47].

The gasification process is controlled by the equivalence ratio (λ), which expresses the actual oxidizer–fuel ratio supplied to the downdraft gasifier in relation to the oxidizer–fuel ratio required for stoichiometric combustion [30], as given by Eq. (1).

$$\lambda = \frac{\left(\frac{\dot{m}_{O_2}}{\dot{m}_f}\right)_{actual}}{\left(\frac{\dot{m}_{O_2}}{\dot{m}_f}\right)_{stoich}} \tag{1}$$

where $\dot{m}_{O_2}$ is the mass flow rate of oxygen in the gasifying agent, and $\dot{m}_f$ is the mass flow rate of biomass feedstock as fuel. A mixture of oxidizer and fuel with $\lambda = 1$ is at stoichiometry;

for fuel-rich mixtures, $\lambda < 1$; and for fuel-lean mixtures, $\lambda > 1$. Hence, complete combustion theoretically occurs at an equivalence ratio equal to unity, where all the carbon in the feedstock is stoichiometrically oxidized to provide the maximum concentration of carbon dioxide in the gaseous product stream. The stoichiometric oxygen requirement is calculated using the data for the ultimate analysis of the biomass feedstock. For a given flow rate of biomass fuel into the downdraft gasifier:

$$\lambda = \frac{(\dot{m}_{O_2})_{actual}}{(\dot{m}_{O_2})_{stoich}} = \frac{(\dot{n}_{O_2})_{actual}}{(\dot{n}_{O_2})_{stoich}} = \frac{\dot{m}_{O_2}\, M_{O_2}^{-1}}{\dot{m}_f \left(\frac{x_{C,f}}{M_C} + \frac{1}{4}\frac{x_{H,f}}{M_H} - \frac{1}{2}\frac{x_{O,f}}{M_O} \right)} \tag{2}$$

where M_{O_2} is the molar mass of oxygen; M_C, M_H, M_O are, respectively, the molar masses of atomic carbon, hydrogen, and oxygen; and $x_{C,f}$, $x_{H,f}$, $x_{O,f}$ are, respectively, the mass fractions of carbon, hydrogen, and oxygen from the ultimate analysis of the feedstock to the gasification process. The expression in Eq. (2) is derived from the complete combustion reaction of a generic solid fuel containing carbon, hydrogen, and oxygen, as shown in Eq. (3).

$$C_aH_bO_c + \left(a + \frac{b}{4} - \frac{c}{2} \right) O_2 \longrightarrow a\, CO_2 + \frac{b}{2}\, H_2O \tag{3}$$

2.2. Producer gas conditioning

The raw producer gas from downdraft gasifiers usually contains tar, ash, soot and other trace contaminants that, if not removed, can lead to severe fouling, erosion and corrosion issues in downstream equipment and compromise the structural integrity of the power generation unit [31, 61]. Gas turbines are particularly sensitive machines with rather stringent restrictions on the producer gas cleaning so as to avoid damage to the turbine blades (such as erosion, incrustation or corrosion) and blockage of filters and fuel injectors. Particulate and tar concentrations in the producer gas should therefore be below 5 mg/Nm^3 [30, 61]. For this reason, a producer gas conditioning unit consisting of a cyclone, a wet scrubber and a series of filters must be included downstream of the gasifier to cool down and clean up the producer gas so that it meets the quality requirements to

be used as fuel by a gas turbine. The cyclone, wet scrubber and filters were modeled with a solid separator (SSplit), a Venturi scrubber gas–solid separator (VScrub), and a gas–liquid separator (Sep), respectively [47]. The conditioned producer gas is then transferred to the power generation unit to be compressed and fueled to the gas turbine combustor [59].

The efficiency of gasification processes is often described by the cold gas efficiency (η_{cg}), which is defined as the efficiency of the gasification process after the producer gas has been cleaned up and cooled down to ambient temperature [30]. It expresses the fraction of the chemical energy flow of the biomass feedstock that remains in the producer gas. Mathematically, this parameter is determined as follows:

$$\eta_{cg} = \frac{\dot{m}_{cg}\,\mathrm{LHV}_{cg}}{\dot{m}_{f}\,\mathrm{LHV}_{f}} \tag{4}$$

where $\dot{m}_{cg}$ and $\dot{m}_{f}$ represent the mass flow rates of conditioned producer gas and biomass feedstock, respectively [30, 47, 49].

2.3. Topping power unit

An internally-fired gas turbine fueled with the conditioned producer gas from biomass gasification is proposed as topping power generation unit. Gas turbines provide a number of potential advantages as compared to other technologies for small-scale power generation [62], such as their compact size and low weight per unit power, low vibration levels and reduced noise, long service life and relatively low maintenance cost due to their small number of moving parts, low emissions of air pollutants and availability of high-grade waste heat [62]. Gas turbines are usually designed and commercialized for gaseous fuels with high energy content such as natural gas or biogas [44]. However, advanced gas turbines for producer gas are also available, most of which were developed and optimized for conventional coal-fueled IGCC plants, with demonstrated operation at numerous sites (e.g., Wabashi River and Tampa in the US, Puertollano in Spain, Buggenum in the Netherlands and Nakoso in Japan) [63]. These advanced gas turbines must incorporate modifica-

tions to the compressor to accommodate the increased mass flow of fuel and also to the combustor to control the increased flame speed as a result of the higher hydrogen content of the producer gas [64–67]. Nevertheless, the main equipment, namely gas turbine and air compressor, can remain virtually unchanged with respect to gas turbines burning standard fuel [67].

The topping power unit consists of a gas turbine that operates on the recuperative Brayton cycle, an improvement over the conventional Brayton cycle that allows for achieving higher efficiencies by recovering some of the waste heat from the exhaust gas [62]. In this topping power unit, the upgraded producer gas from oxygen-enriched air biomass gasification is burned with compressed air in a combustor at constant pressure. The combustion process is modeled as a multiphase equilibrium reactor by minimizing the Gibbs energy of the mixture of both inlet streams to produce the outlet stream [47]. Previously, the producer gas must be brought to the combustor operating pressure by means of a fuel booster compressor [39]. The temperature of the exhaust gas entering the turbine is typically limited to the range of 750–950 °C in recuperative configurations [55, 68, 69], because of technical restrictions on the materials of manufacture. Thus, the turbine inlet temperature is maintained within this range by using excess air. The flow rate of the ambient air stream is controlled by a user-programmed external Fortran statement. The exhaust gas from the combustor at high temperature and pressure expands in the turbine to atmospheric pressure while producing mechanical power. The gas turbine drives the air compressor and the electric generator through a single common shaft [62]. As the electric generator reaches very high rotational speeds (75,000–100,000 rpm), it produces a high-frequency output that must be converted to direct current (DC) and then back to grid-compatible alternating current (AC) through reliable and efficient electronic power conditioning devices [62]. A gas-to-air counter-current heat exchanger known as recuperator is used to transfer thermal energy from the exhaust gas to the already compressed air before it enters the combustion chamber, thereby improving the efficiency of the Brayton cycle. The effectiveness of the recuperator is assumed equal to 87% [70]. Typical values for performance parameters used in the process simulation are reported in Table 1 [44, 55, 56, 68–70].

Table 1: Simulation specifications for the topping power unit based on typical performance parameters.

Equipment	Parameter	Value	Unit
Gas turbine	Isentropic efficiency (η_i)	85	%
	Mechanical efficiency (η_m)	97	%
	Turbine inlet temperature (TIT)	750–950	°C
	Turbine exhaust temperature (T_{eg})	250–300	°C
Generator	Power generation efficiency (η_{gen})	95	%
	Power conversion efficiency, AC/DC/AC (η_{conv})	99	%
Recuperator	Heat transfer effectiveness (ε)	87	%
	Maximum temperature at hot side ($T_{\max}$)	650	°C
Compressors	Isentropic efficiency (η_i)	80	%
	Mechanical efficiency (η_m)	97	%
	Fuel booster electromechanical efficiency (η_{em})	95	%

In the gas turbine industry, the fuel–oxidizer equivalence ratio (ϕ) is often used to characterize the mixing ratio of air and fuel. This parameter refers to the amount of excess air present in the combustion chamber in relation to the amount of air required for stoichiometric combustion, with values below 1 representing excess air and above 1 indicating excess fuel. It is well established that emissions of nitrogen oxides increase with higher temperatures inside the combustion chamber, due to the increasingly higher reactivity of atmospheric nitrogen with increasing temperatures. Nitrogen oxides are air pollutants that contribute to the formation of smog and acid rain, as well as affecting tropospheric ozone. Thus, modern low-emission combustors tend to operate with substantial excess air (i.e., values of ϕ well below 1, down to about 0.1–0.2 in recuperative cycle configurations [66]), in order to avoid reaching the excessively high temperatures responsible for the high rates of nitrogen oxide formation. Furthermore, if turbine inlet temperatures rise above 950 °C, costly materials and complex cooling systems for the turbine blades are required, thereby increasing the capital expenditure and maintenance costs [55, 69]. Moreover, increasing turbine inlet temperatures would also lead to an increase in the temperature of the recuperator, which is typically limited to approximately 600–650 °C due to the use of conventional stainless steel [62, 68–71]. The fuel–oxidizer equivalence ratio is related to the oxidizer–fuel equivalence ratio (defined previously) as follows:

$$\phi = \frac{1}{\lambda} = \frac{\left(\frac{\dot{m}_f}{\dot{m}_{O_2}}\right)_{actual}}{\left(\frac{\dot{m}_f}{\dot{m}_{O_2}}\right)_{stoich}} \tag{5}$$

where $\dot{m}_{O_2}$ is the mass flow rate of oxygen in the air, and $\dot{m}_f$ is the mass flow rate of fuel gas to be burned in the combustion chamber. The airflow rate is adjusted in order to reach a minimum value for λ equal to 6, which means that the actual oxidizer–fuel ratio is at least six times the stoichiometric oxidizer–fuel ratio ($\lambda \geq 6$) [55]. The mass flow rate of air required for stoichiometric combustion is determined by means of the main oxidation reactions that occur in the combustion chamber:

$$2\,CO + O_2 \longrightarrow 2\,CO_2 \tag{6}$$

$$2\,H_2 + O_2 \longrightarrow 2\,H_2O \tag{7}$$

$$CH_4 + 2\,O_2 \longrightarrow CO_2 + 2\,H_2O \tag{8}$$

The net electric power of the topping power cycle is calculated as shown in Eq. (9) by subtracting the power consumed by the compressors from the gross power output of the gas turbine [55].

$$P_{top} = \eta_{conv}\,\eta_{gen}\left(P_{gturb} - P_{comp,shaft}\right) - \frac{P_{comp,boost}}{\eta_{em}} \tag{9}$$

where P_{gturb} and P_{comp} represent the gas turbine and compressors mechanical power, respectively; η_{gen} is the power generation efficiency, η_{conv} is the AC/DC/AC power conversion efficiency and η_{em} is the electromechanical efficiency of the producer gas booster compressor. The main parameters affecting the net power delivered by the gas turbine are the pressure ratio (Π), defined as the ratio of the stagnation pressure at the front and rear of the compressors, and the turbine inlet temperature

(TIT). However, both parameters can only be increased up to certain limits, which depend on material tolerances and the cost of manufacturing. Finally, the net electrical efficiency (η_{top}) of the topping power cycle is calculated with respect to the producer gas consumption, as shown in Eq. (10).

$$\eta_{top} = \frac{P_{top}}{\dot{m}_{cg}\,\mathrm{LHV}_{cg}} \tag{10}$$

2.4. Bottoming power unit

The low-temperature waste heat available in the exhaust gas discharged from the gas turbine can be recovered through a subcritical organic Rankine cycle (ORC) bottoming unit to generate additional power and increase the electrical efficiency of the IGCC plant. In combined cycle power plants based on gas turbines, conventional steam Rankine cycles are typically adopted as bottoming power cycles [72, 73]. However, steam Rankine cycles are not convenient for decentralized power generation in bottoming cycles of smaller size, because of the large and expensive equipment required and the decreased power generation efficiency when operated on a smaller scale. In addition, most modern gas turbines present performance improvements such as high pressure ratios, recuperative cycles or intercooled cycles, at the expense of a lower exhaust gas temperature [72, 73]. As the low-temperature waste heat cannot be effectively exploited with a traditional steam Rankine cycle, the use of organic Rankine bottoming cycles for waste heat recovery from gas turbines characterized by a high efficiency but a low exhaust temperature is an attractive alternative solution [72]. This combination allows for high efficiencies to be achieved, which are similar to those of modern gas and steam combined cycles, but apply to topping cycles with lower turbine inlet temperatures [73]. Organic Rankine cycles are a well-proven technology and already commercially available for small-scale power generation [73, 74]. Moreover, they represent the most feasible solution among all the available small-scale waste heat recovery technologies from a techno-economic standpoint [38, 75].

Conceptually, organic Rankine cycles are operationally similar to conventional steam Rankine cycles in that both are based on the vaporization of a high-pressure liquid, which is in turn expanded to a lower pressure level, thereby releasing mechanical work [74]. However, the main difference is the use of organic working fluids often characterized by a lower boiling point than that of water at the same pressure, which allows the power cycle to be driven by low-grade waste heat [76]. Therefore, organic Rankine cycles involve the same components as a conventional steam power plant. The working fluid is pumped to an evaporator, where it is heated and vaporized under critical conditions, then passed through an expansion device known as expander, which is connected to an electric power generator, and eventually converted back to saturated liquid in the condenser, closing the cycle. Two configurations are typically available for the condenser in organic Rankine cycles: air-cooled or water-cooled condensers. ORC systems with a water-cooled condenser usually have a higher nominal efficiency, due to the lower condensing temperature [77], but also a higher cooling load, which requires a high flow rate of cooling water. The usual constraints on water availability mean that air-cooled condensers are often the preferred choice for most manufacturers of ORC units, and therefore, also the configuration of choice for this work. A realistic value used in this work for the condensation temperature is 45 °C. ORC units can be combined with gas turbines through a thermal oil circuit. Although it is recommended to incorporate a diathermic oil circuit to avoid local overheating and to prevent organic fluids from becoming chemically unstable [78], it is not included in the present work because the exhaust gas temperature is not excessively high and also for the sake of brevity and simplicity [56, 73].

A thoughtful choice of the working fluid is of paramount importance in organic Rankine cycles. The selection of the working fluid affects the thermodynamic cycle, the plant layout, the performance and cost of the equipment, and the safety requirements. From a thermodynamic standpoint, a candidate working fluid should have suitable critical constants, relatively low molecular complexity and a compatible boiling point for the condenser. Working fluids for use in organic Rankine cycles can be classified into three main categories as wet, dry and isentropic depending on their

behavior during adiabatic expansion [79]. Dry or isentropic working fluids do not condense during expansion from a saturated state, and thus, do not require superheating, thereby eliminating the concerns of impingement of liquid droplets on the expander blades [80, 81]. Nevertheless, if the saturated vapor curve of the dry fluid sharply deflects inward, the vapor will exit from the expander with a significant degree of superheat. Therefore, if dry working fluids are used, a regenerative cycle configuration is typically adopted to increase the thermodynamic efficiency of the organic Rankine cycle and avoid unnecessarily adding to the condenser cooling load [80]. Regenerative organic Rankine cycles incorporate a counter-current heat exchanger called regenerator in order to recover the heat from the exiting superheated vapor at the expander outlet by preheating the pressurized organic fluid before the evaporator [80].

As indicated in the available guidelines for selection of the working fluid in organic Rankine cycles [78–83], the following additional key factors should be considered: commercial availability at a reasonable specific cost, flammability, toxicity, chemical stability at high temperatures and environmental factors, such as ozone depletion potential (ODP) and global warming potential (GWP). Since no single working fluid is likely to be able to meet all of the preferred standards, a trade-off approach to choice should prevail. Five dry working fluids have been considered in this work, namely pentane (*n*-C5 or R601), isopentane (*i*-C5 or R601a), cyclopentane (*c*-C5), pentafluoropropane (R245fa) and trans-1-chloro-3,3,3-trifluoropropene (R1233zd), according to the following selection criteria: suitability for the waste heat source and sink temperatures, molar mass, critical constants and environmental, health and safety aspects. Table 2 presents a summary of the physicochemical and environmental properties of these organic fluids [81, 83, 84]. None of the proposed working fluids are ozone-depleting, but some present significant global warming potential. The maximum operating temperature of the selected working fluids is 300 °C, which corresponds to the thermochemical stability temperature limit beyond which their thermal decomposition increases significantly [85]. In addition, the pressures in the condenser were always considered close to or higher than the ambient pressure to avoid air leakages into the organic working

fluid circuit [79], which restricts the use of other popular dry working fluids in organic Rankine cycles such as cyclohexane, benzene or toluene. The final choice of the most suitable working fluid is made in accordance with the following performance parameters: highest net electrical efficiency of the bottoming unit, highest thermodynamic efficiency of the organic Rankine cycle, lowest environmental impact of the working fluid and highest value of the figure of merit ($\Delta h/v_g$). This last parameter represents the amount of heat transferred per unit volume in the condenser [86, 87]. Therefore, the higher the figure of merit, the greater the amount of heat exchanged per unit volume and the smaller the condenser can be. The value of the figure of merit for the various fluids is also included in Table 2. It is worth noting that this figure of merit does not refer to the actual heat transfer area, but rather to the volume of the condenser.

Table 2: Physicochemical and environmental properties of the candidate working fluids for the organic Rankine cycle.

Organic fluid	**Molar mass**	**Critical constants**		**Boiling point**	**Figure of merit**	**Environmental issues**[a]			
	M (g/mol)	p_c (bar)	T_c (°C)	T_b (°C) at 1 atm	$\Delta h/v_g$ (kJ/m^3) at 45 °C	GWP_{100}[b]	H	F	I
n-C5	72.15	33.7	196.7	36.1	1375	4–6	1	4	0
i-C5	72.15	33.8	187.3	27.8	1701	4–6	1	4	0
c-C5	70.13	45.1	238.5	49.2	944	4–6	1	3	0
R245fa	134.05	36.5	154.0	15.1	2938	1030	2	1	0
R1233zd	130.50	36.2	166.5	18.3	2445	1	2	0	0

[a] Safety information according to the hazard rating system by the National Fire Protection Association (NPFA) of the United States. Each of the health (H), flammability (F) and instability (I) hazards is rated on a scale from 0 (no hazard) to 4 (severe hazard).
[b] GWP_{100}: Global warming potential in a 100-year period.

The performance parameters and technical restrictions of the regenerative organic Rankine cycle are reported in Table 3 [56, 73]. The heat exchangers are designed with a minimum pinch point temperature difference (ΔT_{pinch}) of 10 °C [56, 87, 88]. The maximum working pressure is limited to 20 bar to ensure a safe operation and reduce material costs [56, 81]; while the maximum evaporation temperature is constrained to 10 °C below the critical temperature of the working fluid to avoid thermal instability [56]. The minimum temperature of the off-gas leaving the evaporator must be at least 100 °C in order to prevent corrosion and undesirable condensates in pipelines and mechanical equipment [39, 56].

Table 3: Simulation specifications for the bottoming power unit based on typical performance parameters.

Equipment	**Parameter**	**Value**	**Unit**
Expander	Isentropic efficiency (η_i)	80	%
	Mechanical efficiency (η_m)	95	%
Generator	Power generation efficiency (η_{gen})	95	%
Evaporator	Heat source temperature (T_{eg})	250–300	°C
	Minimum pinch point temperature difference (ΔT_{pinch})	10	°C
	Minimum temperature of the off-gas (T_{og})	100	°C
Condenser	Condensation temperature (T_{cond})	45	°C
Regenerator	Heat transfer effectiveness (ε)	90	%
	Minimum pinch point temperature difference (ΔT_{pinch})	10	°C
Pump	Maximum operating pressure ($p_{\max}$)	20	bar
	Electromechanical efficiency (η_{em})	95	%
	Isentropic efficiency (η_i)	70	%
	Mechanical efficiency (η_m)	97	%

The thermodynamic efficiency of the ORC bottoming power cycle is defined as given by the following equation:

$$\eta_{\text{ORC}} = \frac{P_{exp} - P_{pump}}{\dot{m}_{wf}\,\Delta h_{evap}} \tag{11}$$

where P_{exp} and P_{pump} respectively represent the mechanical power of the expander and the pump, $\dot{m}_{wf}$ is the mass flow rate of organic working fluid and Δh_{evap} is the enthalpy increase of the working fluid in the evaporator [56].

The net electric power of the organic Rankine bottoming power cycle is calculated as shown in Eq. (12) by subtracting the electric power consumed by the pump from the gross electrical power output.

$$P_{bottom} = \eta_{gen}\,P_{exp} - \eta_{em}\,P_{pump} \tag{12}$$

where η_{gen} is the electrical efficiency of the generator and η_{em} is the electromechanical efficiency of the pump [56].

The net electrical efficiency of the ORC bottoming power unit is eventually determined as follows:

$$\eta_{bottom} = \frac{P_{bottom}}{\dot{m}_{eg}\, c_{p,eg} \left(T_{eg} - T_a\right)} \tag{13}$$

where $\dot{m}_{eg}$ is the mass flow rate of exhaust gas from the gas turbine, $c_{p,eg}$ is the mass heat capacity of the exhaust gas, T_{eg} is the temperature of the exhaust gas and T_a is the ambient temperature.

2.5. Alkaline water electrolysis

The alkaline electrolyzer is powered by the electricity produced in the IGCC. When a suitable electric potential is applied to the electrodes of an alkaline water electrolysis cell, the following half-cell reactions occur [8, 13, 14, 17].

$$\text{Cathode: } 2\,H_2O\,(l) + 2\,e^- \longrightarrow H_2\,(g) + 2\,OH^-\,(aq) \tag{14}$$

$$\text{Anode: } 2\,OH^-\,(aq) \longrightarrow \frac{1}{2}\,O_2\,(g) + H_2O\,(l) + 2\,e^- \tag{15}$$

Deionized water is introduced into the cathode of the alkaline electrolysis cell, where it is reduced to give hydrogen and hydroxide anions by means of a direct electric current. The negatively charged ions then travel through the electrolyte to the anode, where oxygen is formed. The two-phase mixtures of liquid electrolyte and gaseous product then leave the electrolysis stack on each side and enter subsequent flash separators. The liquid electrolyte is eventually cooled down and pumped back to the electrolysis stack, while the gaseous hydrogen and oxygen products are demisted and purified to the desired level [8]. The minimum voltage required for water splitting or reversible cell voltage (V_{rev}) is defined by the next equation:

$$V_{rev} = \frac{\Delta G}{z\,F} \tag{16}$$

where ΔG is the change in the Gibbs free energy, z is the number of electrons transferred per hydrogen molecule and F is the Faraday constant (96 485 A·s/mol) [8]. The reversible cell voltage corresponds to 1.23 V at SATP conditions (1 bar and 25 °C) [8, 10]. However, the alkaline electrolysis cell requires the input of an amount of energy equal to the enthalpy of reaction (ΔH), which is the sum of the Gibbs free energy (ΔG) and the thermal energy through the term $T\Delta S$ [13]. If both amounts are supplied in the form of electrical energy, the reversible cell voltage increases with the so-called thermal voltage, leading to the thermoneutral voltage (V_{tn}), as shown in Eq. (17). The thermoneutral cell voltage is 1.48 V at SATP conditions [13].

$$V_{tn} = \frac{\Delta H}{z\,F} = \frac{\Delta G + T\,\Delta S}{z\,F} \tag{17}$$

The thermoneutral voltage represents the standard operation mode of high-temperature electrolyzers. By contrast, low-temperature electrolyzers such as alkaline electrolyzers are operated at a cell voltage above the thermoneutral voltage ($V_{cell} > V_{tn}$), due to high internal losses or overvoltages [13], which typically increase when the water electrolysis process is operated at higher current densities. The power requirement of the alkaline electrolysis stack (P_{stack}) is given by:

$$P_{stack} = N\,i\,A_{cell}\,V_{cell} \tag{18}$$

where N is the number of cells in series of the electrolysis stack, V_{cell} is the cell voltage, A_{cell} is the active electrode area and i is the current density [10]. The molar rate of hydrogen production ($\dot{n}_{\mathrm{H_2}}$) is eventually calculated as follows:

$$\dot{n}_{\mathrm{H_2}} = \eta_F \frac{P_{stack}}{V_{cell}\,z\,F} = \eta_F \frac{N\,i\,A_{cell}}{z\,F} \tag{19}$$

where η_F is the Faraday efficiency [10, 11], which is defined as the ratio of actual to theoretical hydrogen production rate [13].

Aspen Plus does not include any in-built block unit to represent an electrolysis cell stack [10],

and thus, a combination of several blocks is required to model the water electrolysis process. The alkaline electrolysis stack is modeled within a hierarchy block, which uses the NRTL (Non-Random Two-Liquid) model as property method [10]. The hierarchy block includes a stoichiometric reactor (RStoic), several flash separators (biphasic separators and water traps), in addition to BOP equipment such as circulation pumps and a cooling fan [10]. The power requirement of the stack is entered as heat [10]. The performance parameters used in the process simulation are reported in Table 4 [10, 26, 89]. In addition, the following assumptions are considered to simplify the simulation process:

- The power conversion efficiency from alternating current (AC) to direct current (DC) in the rectifier is assumed at 98% [13, 26].
- Liquid deionized or demineralized water is fed to the system under SATP conditions [9, 10].
- The electrolyte is an aqueous potassium hydroxide (KOH) solution at a concentration of 35% by weight [10, 12]. A relatively high concentration of KOH in the electrolyte ensures high conductivity and contributes to reducing the ohmic overpotential [10].
- The operating temperature of the alkaline electrolyzer has a strong influence on performance, but it is limited by degradation issues of the electrolysis cells and material restrictions. Alkaline electrolyzers are operated at temperatures between 60–90 °C [5, 7, 10, 13, 14]. A typical value within this range is 70 °C [10, 89]. Both hydrogen and oxygen are discharged from the electrolyzer at ambient temperature [10]. About 10% of the total heat produced by the stack is released to the environment as convection and radiation heat losses [10].
- The alkaline electrolysis stack operates at a pressure of 16 bar, in accordance with other systems of a similar size range [89]. Operating the electrolysis process at higher pressures than the ambient pressure is often regarded as convenient, because the power demanded by the downstream hydrogen compressor is reduced [9, 13]. However, an operating pressure above 30–50 bar would require additional safety devices and result in higher complexity

and investment costs [5, 13, 14]. The electrolysis stack is operated at balanced anode and cathode pressure [10]. A 5% pressure drop is assumed to occur in the flash separators [10].

- At nominal current density, the Faraday efficiency of alkaline water electrolyzers is reported to be close to 100% (98–99.9%) [13]. Thus, in this work, the Faraday efficiency is assumed to be $\eta_F = 99\%$, roughly the average value.
- Commercial electrolyzers typically reach current densities up to 0.45 A/cm^2 [7, 13, 90]. The cell voltage at a nominal current density of 0.4 A/cm^2 varies between 1.7–2.1 V [13]. An average value of 1.9 V is assumed for the cell voltage in this work [13], which agrees with the expected values from the polarization curves of commercial alkaline electrolyzers under equivalent conditions of temperature and pressure [10, 13, 89].
- Hydrogen has a very low density and high pressures are needed to store it within a reasonable volume [9]. Therefore, the hydrogen output is eventually compressed up to 200 bar for bulk gaseous storage in high-pressure vessels [91–93]. Compression of the hydrogen output for storage must be considered with care, as it is a highly energy-intensive operation [92]. In multistage compressors, the compressed hydrogen is cooled down after each stage to make compression less adiabatic and more isothermal, thereby reducing the energy requirement for compression [93]. It is well established that the higher the number of compression stages, the higher the efficiency, but also the higher the number of parts and complexity of the compressor, as well as the cost to purchase, service, and maintain the equipment. Thus, a three-stage hydrogen compression unit with intercooling and aftercooling is used in this work [9], because it represents a trade-off between efficiency and cost.

The efficiency of low-temperature electrolyzers is often given based on the higher heating value (HHV) of hydrogen, which corresponds to the enthalpy of reaction at standard conditions from liquid water to gaseous hydrogen [13]. However, for evaluation of an overall process chain, the partial efficiencies of unit operations are usually referred to the lower heating value (LHV) [13]. Accordingly, the efficiency of the alkaline electrolysis stack (η_{stack}) is referred to the lower

Table 4: Simulation specifications for the alkaline water electrolyzer based on typical performance parameters.

Equipment	Parameter	Value	Unit
Rectifier	AC/DC conversion efficiency (η_{conv})	98	%
Electrolyzer	Stack operating temperature	70	°C
	Stack operating pressure	16	bar
	Electrolyte concentration	35	%
	Nominal current density	0.40	A/cm^2
	Cell voltage	1.9	V
	Faraday efficiency (η_F)	99	%
Pumps	Electromechanical efficiency (η_{em})	95	%
	Isentropic efficiency (η_i)	70	%
	Mechanical efficiency (η_m)	90	%
Hydrogen compressor	Number of stages	3	
	Isentropic efficiency (η_i)	72	%
	Output pressure	200	bar

heating value as follows:

$$\eta_{stack} = \frac{\dot{m}_{\mathrm{H_2}}\,\mathrm{LHV}_{\mathrm{H_2}}}{P_{stack}} = \frac{\dot{m}_{\mathrm{H_2}}\,\mathrm{LHV}_{\mathrm{H_2}}}{\eta_{conv}\left(P_{top} + P_{bottom} - P_{\mathrm{BOP}} - P_{comp}\right)} \tag{20}$$

where η_{conv} is the AC/DC conversion efficiency, P_{BOP} is the parasitic power consumption by the utilities (deionized water supply, heat exchangers, gas-liquid separator vessels, circulation pumps, and the cooling loop) that are part of the BOP equipment, and P_{comp} is the power required for hydrogen compression. The total power required by the BOP equipment is estimated at approximately 8% of the net power input [10, 89]. The net efficiency of the alkaline electrolytic hydrogen production and compression unit (η_{AWE}) is eventually determined as shown in Eq. (21), which includes the power consumed by the hydrogen compressor and all the utilities that make up the BOP equipment.

$$\eta_{\mathrm{AWE}} = \frac{\dot{m}_{\mathrm{H_2}}\,\mathrm{LHV}_{\mathrm{H_2}}}{P_{top} + P_{bottom}} \tag{21}$$

Under part-load operation of the alkaline electrolyzer, the efficiency of the stack based on the LHV (η_{stack}) typically increases, as a consequence of the reduction in the cell overvoltages

at lower current densities [10, 13]. However, decreasing the Faraday efficiency (η_F), relatively increasing the specific consumption of utilities (BOP) and substantially reducing the utilization factor carry a large penalty for the overall performance of the water electrolysis process [13]. Thus, the electrolyzer is intended to operate continuously at nominal load with an availability of at least 98%, because it reduces the share of parasitic losses and provides a very high utilization factor that maximizes the annual production of hydrogen.

2.6. Overall energy balance

As mentioned above, for evaluation of the overall performance of the IGCC-AWE plant, the partial efficiencies are referred to the LHV of the biomass feedstock. Accordingly, the gross electrical efficiency (η_{IGCC}) of the IGCC is defined with respect to the chemical energy flow in the biomass feedstock consumed by the hybrid IGCC-AWE plant [39], as given by Eq. (22).

$$\eta_{\text{IGCC}} = \frac{P_{top} + P_{bottom}}{\dot{m}_f \, \text{LHV}_f} \tag{22}$$

Finally, by considering the hybrid IGCC-AWE plant as a whole, the overall energy efficiency ($\eta_{\text{IGCC-AWE}}$) is defined as the ratio in terms of energy flow between the rate of hydrogen production and the total consumption of biomass feedstock.

$$\eta_{\text{IGCC-AWE}} = \frac{\dot{m}_{\text{H}_2} \, \text{LHV}_{\text{H}_2}}{\dot{m}_f \, \text{LHV}_f} = \eta_{\text{IGCC}} \, \eta_{\text{AWE}} \tag{23}$$

3. Results and discussion

In this section, the results of the process simulations are presented and discussed in order to evaluate the performance of the proposed hybrid IGCC-AWE plant for continuous decentralized hydrogen production from biomass operating under steady-state conditions. All the unit operations and streams included in the hybrid IGCC-AWE plant were sized considering that the downdraft gasifier is supplied with dry woody biomass pellets (6% moisture content, wet basis) at a constant

mass flow rate of 1 t/h. The yield of oxygen from alkaline water electrolysis is about 8 kg per each kg of hydrogen, which is not enough to fire the downdraft gasifier with pure oxygen in an energy self-sufficient hydrogen production approach. Thus, oxygen-enriched air is used to obtain an upgraded producer gas with a moderately increased calorific value compared to the lean producer gas from gasification using ambient air as gasifying agent. The hybrid system is designed to supply all the oxygen by-produced by the alkaline electrolyzer to the downdraft gasifier in order to produce the upgraded producer gas, which is fueled to a combined cycle power plant. The net power generation output is used to continuously produce renewable hydrogen in the alkaline electrolyzer.

3.1. Biomass gasification and producer gas conditioning

The capacity of downdraft gasifiers is typically limited to ~500 kg/h, due to the physical constraints of the gasifier diameter to particle size ratio [31]. Downdraft gasifiers blown with ambient air as gasifying agent are often sized for a feedstock consumption of 0.1–0.7 t/h [31]. However, if downdraft gasifiers are fired with oxygen, their capacity can increase up to 1–5 t/h [31]. Since oxygen-enriched air is proposed as gasifying agent rather than pure oxygen, the downdraft gasifier can be sized for a feedstock consumption of ~1 t/h. Worthy of note is that downdraft gasifiers can be scaled up for a slightly larger capacity in case of using oxygen-enriched air instead of ambient air as gasifying agent, as a result of the decreasing flow rate of the energy-denser producer gas with increasing concentrations of oxygen in the gasifying agent.

It is well-established that the most important operating parameter in autothermal gasification processes is the equivalence ratio (λ), since it controls the temperature inside the gasifier, and affects the yield and composition of the producer gas [49]. The value of λ should be high enough to reach a sufficiently high temperature (~1000 °C) inside the gasifier to minimize tar formation [49]. Accordingly, the value of λ must be adjusted to reach a reaction temperature of 1000 °C in the multiphase equilibrium reactor that models the oxidation and reduction reactions [56]. It is noteworthy that when heat losses are accounted for in the thermodynamic equilibrium calcu-

lations, a higher value of λ is required to reach a certain temperature in the gasifier compared to the adiabatic case [49]. However, increasing the value of λ also leads to higher amounts of combustion products such as carbon dioxide and water vapor, in addition to a larger presence of inert gases such as nitrogen and argon in the producer gas composition. An excessive increase in the value of λ ultimately results in a very lean fuel gas, which is not suitable for power generation. In this regard, the use of oxygen-enriched air instead of ambient air as gasifying agent can be an alternative solution for reaching sufficiently high temperatures inside the gasifier to ensure a low tar content in the producer gas, while increasing its calorific value by substantially reducing the nitrogen dilution effect. In the hybrid IGCC-AWE plant, the oxygen concentration in the oxygen-enriched air used to fire the downdraft gasifier is conditional on the supply of electrolytic oxygen from the alkaline water electrolyzer, which in turn depends on the power generation performance of the combined cycle if there is no external power supply. Thus, the oxygen concentration in the gasifying agent can only be increased up to a certain extent, namely up to a maximum concentration of approximately 35% by volume, as will be demonstrated later. In other words, a maximum of about 0.20–0.25 kg of electrolytic oxygen can be supplied to the downdraft gasifier per each kg of input biomass depending on the equivalence ratio and the physicochemical properties of the biomass feedstock (proximate and ultimate analyses).

Fig. 3 shows the effect of increasing the oxygen concentration in the gasifying agent on the temperature inside the gasifier, the lower heating value of the producer gas and the cold gas efficiency for several values of λ. It can be observed that higher concentrations of oxygen in the gasifying agent allow reducing the value of λ required to reach a certain temperature inside the downdraft gasifier, while leading to a substantial increase in the calorific value of the producer gas. By contrast, higher values of λ allow reducing the oxygen concentration required to reach a certain temperature inside the downdraft gasifier, but also involve a decrease in the calorific value of the producer gas. In the range of oxygen concentrations from 20.75% to 35% by volume, the value of λ must be at least 0.32 in order to reach a temperature above 1000 °C, considering 7% of heat

losses to the environment based on the chemical energy flow of biomass [49, 56]. Interestingly, the cold gas efficiency (η_{cg}) is virtually unaffected by the increase in the oxygen concentration in the gasifying agent, because the increasing calorific value of the producer gas is compensated by the decreasing yield of this gaseous fuel. However, the lower the value of λ, the higher the cold gas efficiency, which is not surprising, since it involves further oxidation of the biomass feedstock toward stoichiometric combustion.

In pursuance of a temperature of 1000 °C inside the downdraft gasifier to ensure a low tar content in the producer gas composition and maximize the cold gas efficiency, the value of λ was adjusted to 0.32 for an oxygen concentration in the oxygen-enriched air equal to 33%. The required consumption of oxygen by-product from the water alkaline electrolyzer is about 0.14 Nm^3 per kg of biomass feedstock. Under such conditions, the yield of clean upgraded producer gas is 1.78 Nm^3/kg, with the following molar composition (%, dry basis): 29.1% CO, 17.6% H_2, 5.2% CH_4, 13.7% CO_2, 34.0% N_2 and 0.4% Ar. Accordingly, the lower heating value (LHV) of the upgraded producer gas is 7.45 MJ/Nm^3, and the cold gas efficiency (η_{cg}) is equal to 74.4%. A slightly higher concentration of oxygen in the gasifying agent (~35%) is conducive to an upgraded producer gas with an LHV close to 8 MJ/Nm^3. This means an increase in the energy density of the upgraded producer gas of more than 50% or even almost double with respect to the producer gas from gasification using ambient air as gasifying agent. However, no further energy enhancement of the producer gas is possible with the current approach.

In order to tune and validate the modified thermodynamic equilibrium model of the downdraft gasifier, the predictions were compared with the experimental results of Cheng et al. [94]. This work reports the measured composition and calorific value of the producer gas from biomass gasification using different mixtures of oxygen-enriched air as gasifying agent. In their experiments, an autothermal gasifier was operated at atmospheric pressure and a constant equivalence ratio of λ = 0.37, while the oxygen concentration in the gasifying agent was varied from 21% to 31.4% by volume, which led to a remarkable increase in the LHV of the producer gas from 4.4 MJ/Nm^3

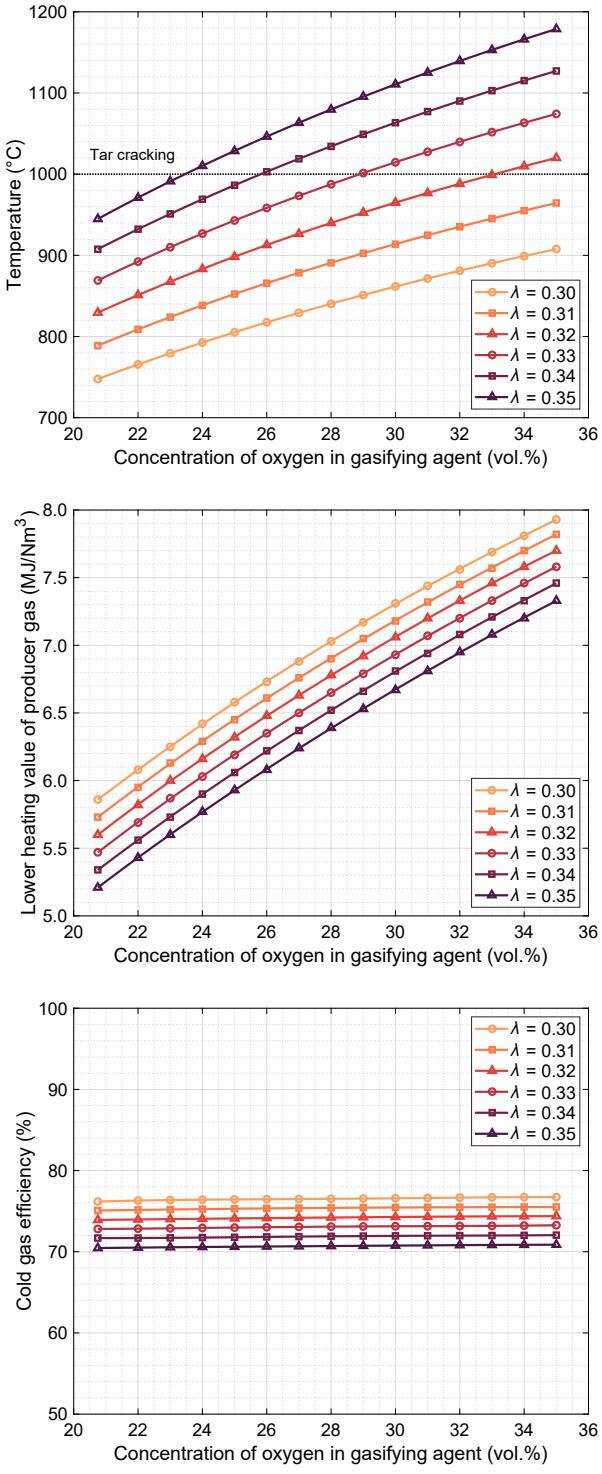

Figure 3: Temperature inside the downdraft gasifier (*top*), lower heating value of the producer gas (*center*) and cold gas efficiency (*bottom*) as a function of the oxygen concentration in the gasifying agent and the equivalence ratio.

to 6.2 MJ/Nm^3 [94], i.e. an increase of just over 40%. As it can be seen in Fig. 4, the predicted values for the most abundant species in the producer gas and the LHV present relatively small deviations with respect to the actual measured values. The largest experimental discrepancies were noticed for the concentration of carbon dioxide, which was moderately overestimated. This might be due to the presence of significant amounts of other gaseous products than those considered in the model, especially at lower concentrations of oxygen in the gasifying agent. However, the LHV of the producer exhibited a reasonably good agreement, with relative prediction errors below 10%, which become negligible for the cases of higher concentrations of oxygen in the gasifying agent.

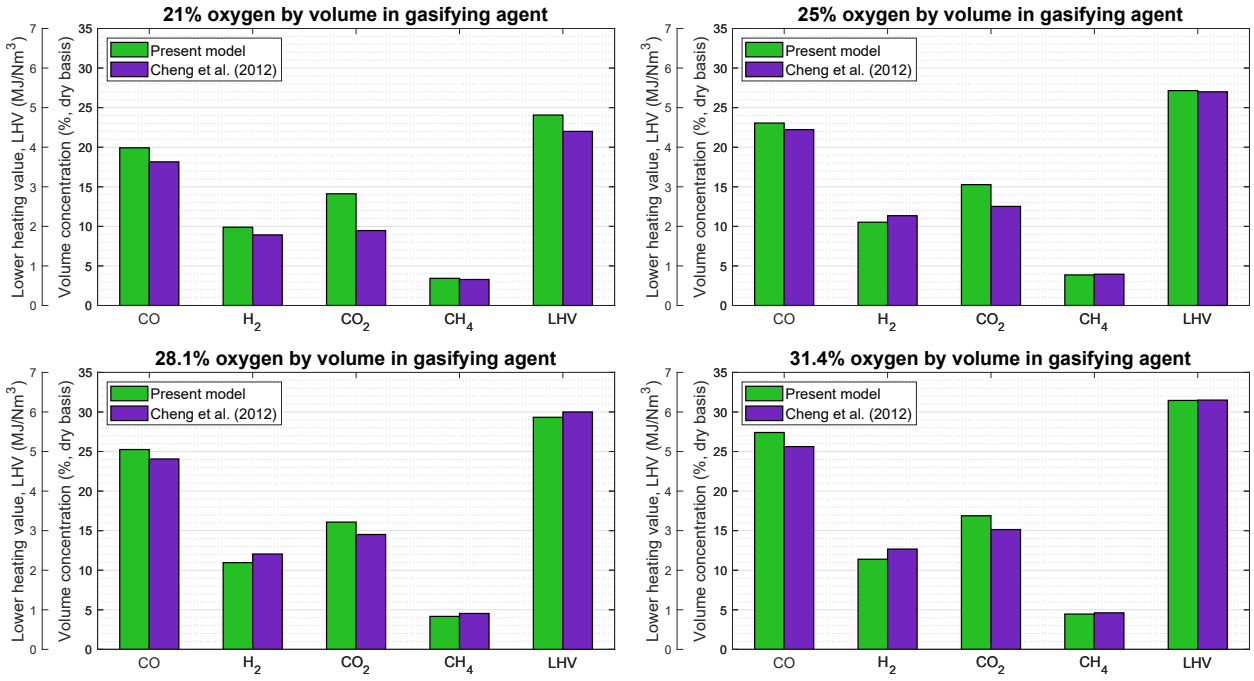

Figure 4: Validation of the present model for oxygen-enriched air biomass gasification with the experimental results of Cheng et al. [94].

3.2. Topping power unit

The main operating parameters of the gas turbine fueled with the conditioned producer gas, such as the compressor pressure ratio (Π), turbine inlet temperature (TIT) and equivalence ratio (ϕ) were evaluated in order to maximize the net electrical efficiency of the topping power unit (η_{top}).

Fig. 5 illustrates the effect of the compressor pressure ratio on the net electrical efficiency of the topping power unit for several turbine inlet temperatures ranging from 750 °C to 1000 °C. It can be observed that for each turbine inlet temperature, the net electrical efficiency of the topping power unit initially increases rapidly with increasing values of Π until reaching a maximum value, and then progressively decreases at a slower rate with further increase of Π. This is because increasing values of Π lead to varying increments in the power generated by the turbine and the power required by the air compressor in the common shaft, as well as the power consumed by the booster compressor. At lower values of Π, the increment of power generated by the turbine is leading, and therefore, the net power increases. By contrast, at higher values of Π, the increment of power required by both compressors takes the lead, and thus, the net power decreases. Higher turbine inlet temperatures lead to higher electrical efficiencies at all values of Π. As shown in Fig. 5, the maximum values for the net electrical efficiency of the topping unit in the range of turbine inlet temperatures from 750 °C to 1000 °C are found for pressure ratios between 2.6 and 3.7.

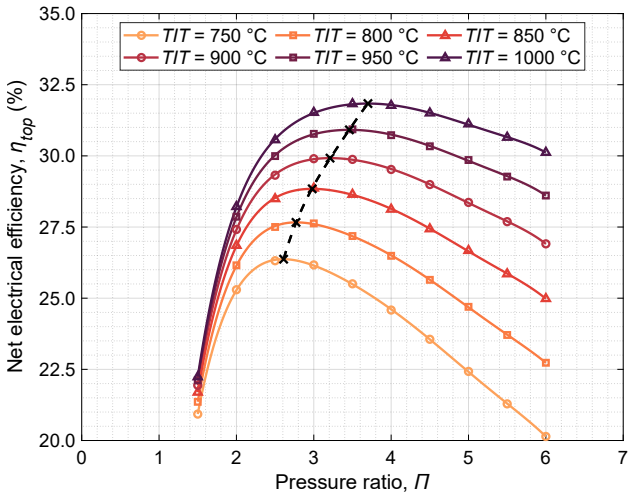

Figure 5: Effect of the pressure ratio and turbine inlet temperature on the net electrical efficiency of the topping power unit. The peak performance curve is represented by the dashed black line.

The performance of the topping power unit fueled with the upgraded producer gas is improved with respect to the case of using lean producer gas from air-blown gasification as fuel. This is due to the higher calorific value and lower volumetric flow rate of the upgraded producer gas, which

significantly reduces the power consumption in the booster compressor, thereby increasing the net electrical efficiency of the topping power unit.

As the temperature limit of the turbomachinery material is about 1000 °C, the turbine inlet temperature is eventually adjusted to 950 °C by setting the value of the air–fuel equivalence ratio (λ) at 7.77, which corresponds to a fuel–air equivalence ratio (ϕ) of 0.1287. The pressure ratio is adjusted to 3.5, which, as evidenced in Fig. 5, provides the optimal conditions at that turbine inlet temperature, leading to a net electrical efficiency of just under 31%. The inlet pressure to the compressors is considered equal to the ambient pressure of 1 bar under SATP conditions, while the outlet pressure is adjusted to reach the optimal performance at the given turbine inlet temperature (TIT). Under these optimal operating conditions, the fuel booster compressor consumes approximately 10% of the gross electric power output of the topping power unit. The recuperator is designed for a constant heat transfer effectiveness of 87%, as reported earlier in Table 1. The maximum temperature in the recuperator is 620 °C, which is below the temperature limit of conventional stainless steel (~650 °C) [68–71]. The temperature of the exhaust gas from the recuperative gas turbine is about 290 °C.

3.3. Bottoming power unit

The performance of the organic Rankine cycle exhibits significant variability depending on the working fluid used. Fig. 6 presents, for each of the above-mentioned working fluids, the thermodynamic efficiency of the organic Rankine cycle (η_{ORC}) and the net electrical efficiency of the bottoming power unit (η_{bottom}) as a function of the pressure in the evaporator (p_{evap}) for different temperatures at the expander inlet (TIT). As expected, the thermodynamic efficiency of the organic Rankine cycle always increases with higher pressures in the evaporator and higher temperatures at the expander inlet. However, the net electrical efficiency of the bottoming unit follows different trends for each working fluid. The constraints on minimum pinch point temperature difference in the evaporator and minimum temperature of the off-gas mean that for some working fluids (i.e., *n*-C5, *i*-C5 and *c*-C5), the net electric power, and therefore also the net elec-

trical efficiency, are higher at lower expander inlet temperatures. By contrast, working fluids such as R245fa and R1233zd are not constrained by the minimum pinch point temperature difference in the evaporator over the range of operating conditions examined, so the net electrical efficiency follows a similar trend to that of the thermodynamic efficiency. The optimal configuration of the bottoming power cycle for each working fluid is also displayed in Fig. 6.

Table 5 reports the optimal performance parameters of the bottoming power unit for the different working fluids considered. It can be observed that *c*-C5 exhibits the highest net electrical efficiency, with a maximum value of 13.2%; followed by *n*-C5, *i*-C5, R1233zd and R245fa. The same descending order of the working fluids is also observed in terms of their corresponding critical temperatures, which in turn limit the optimal expander inlet temperatures. It is noteworthy that almost all of these working fluids condense above ambient pressure at 45 °C, with the sole exception of *c*-C5. Operation of the condenser under vacuum can cause air leakages into the working fluid circuit, although a vacuum of only 0.89 bar for the case of *c*-C5 can be regarded as acceptable. As a result of its relatively low density, a remarkable disadvantage of *c*-C5 is its comparatively lower value for the figure of merit ($\Delta h/v_g$), which will require using a larger condenser (see Table 2).

Table 5 also shows that the working fluid with the lowest mass flow rate is *c*-C5, followed by *n*-C5 and *i*-C5, while those with the highest flow rate are the heaviest fluids, namely R1233zd and R245fa. As a result of their comparatively higher mass flow rates, the highest pump power consumptions (P_{pump}) are produced for R245fa and R1233zd. Saturated aliphatic hydrocarbons such as *n*-C5 and *i*-C5 are highly flammable, which is why they are often avoided in favor of other fluids such as R245fa or R1233zd for safety reasons, despite the fact that they require the highest mass flow rate and pump power consumption. However, using a non-flammable working fluid (e.g., R245fa vs. *n*-C5) leads to a fluid cost at least 12 times higher than that of using a flammable fluid, with a relevant impact on power block economics [83]. On the other hand, the use of flammable fluids requires additional safety protection. Somewhere in between in terms of flammability lies

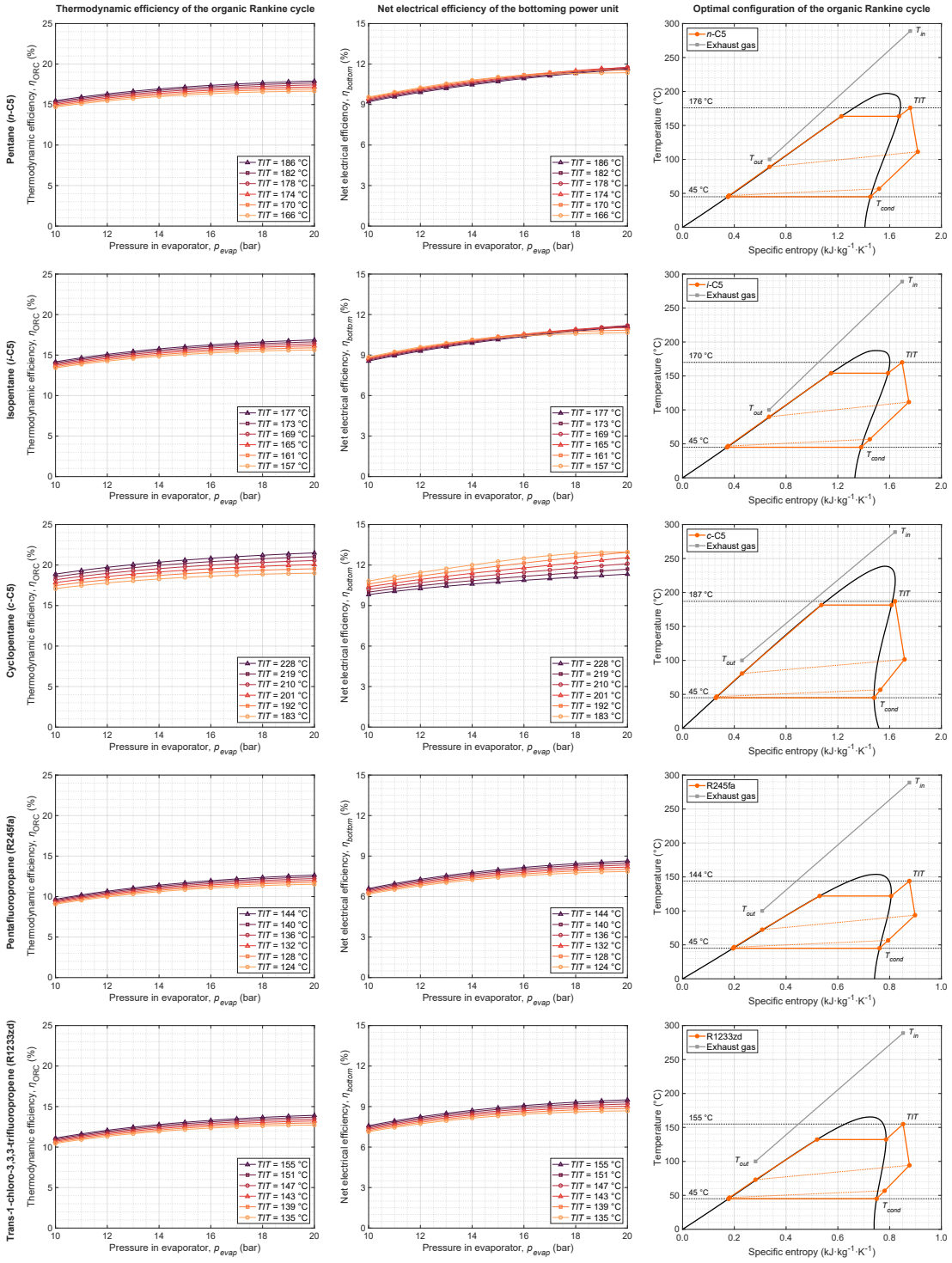

Figure 6: Optimization of the bottoming power unit for each organic working fluid: thermodynamic efficiency of the organic Rankine cycle (*left*), net electrical efficiency of the bottoming power unit (*center*) and optimal configuration of the bottoming power cycle (*right*).

c-C5, a moderately flammable alicyclic hydrocarbon, although with a lower flammability rating than those of *n*-C5 and *i*-C5 in the NFPA 704 safety standard. Aliphatic hydrocarbons (i.e., *n*-C5, *i*-C5 and *c*-C5) also present a relatively low GWP, in contrast to R245fa, which is a hydrofluorocarbon with a GWP of approximately 1030 likely to be phased out in the near future, because of its significant impact to climate change [95]. R1233zd was proven as an appropriate drop-in replacement to R245fa, with similar thermodynamic properties and an extremely low GWP [95]. However, these last two working fluids are rated as more hazardous to human health than aliphatic hydrocarbons in the NFPA 704 safety standard.

In light of the results from the comparative analysis, it can be concluded that *c*-C5 is the working fluid with the best overall performance, and hence, also the working fluid of choice for the purpose of this work.

Table 5: Optimal performance parameters of the organic Rankine cycle for each of the working fluids.

Performance parameter	**Organic working fluid**				
	***n*-C5**	***i*-C5**	***c*-C5**	**R245fa**	**R1233zd**
Pressure in evaporator, p_{evap} (bar)	20	20	20	20	20
Pressure in condenser, p_{cond} (bar)	1.36	1.76	0.89	2.92	2.51
Expander inlet temperature, TIT (°C)	176	170	187	144	155
Minimum approach temperature (°C)	10.0	10.0	10.0	27.6	26.9
Mass flow rate per net power output, $\frac{\dot{m}_{wf}}{P_{bottom}}$ (kg/kWh$_e$)	48	54	39	136	121
Pump power consumption, $\frac{P_{pump}}{P_{exp}}$ (% on gross power output)	6.4	6.9	4.4	7.7	7.5
Thermodynamic efficiency, η_{ORC} (%)	17.3	16.5	19.2	12.7	13.2
Net electrical efficiency, η_{bottom} (%)	11.8	11.2	13.2	8.6	9.5

3.4. Alkaline water electrolysis and hydrogen compression

The efficiency of the alkaline water electrolyzer referred to the LHV of hydrogen lies within the usual range of 50–70% for commercial systems [7, 13, 21, 90]. At the design cell voltage of 1.9 V and nominal current density of 0.4 A/cm^2, the stack efficiency (η_{stack}) is 65.4% and the net system efficiency (η_{AWE}) is 60.2%. The difference between both values represents the power consumption of the BOP equipment, which reduces the net system efficiency considerably [10]. The

alkaline water electrolysis stack consumes 51.0 kWh of electrical energy per kilogram of hydrogen output (i.e., a specific energy consumption of 51.0 kWh/kg). This value is in agreement with the range of 47–66 kWh/kg reported by IRENA for the specific energy consumption of state-of-the-art alkaline water electrolysis stacks [15]. In terms of volume, the energy consumption of the alkaline water electrolysis stack per normal cubic meter (Nm^3) of hydrogen is 4.6 kWh, which lies within the usual range of 4.2–4.8 kWh/Nm^3 reported for commercial alkaline water electrolysis stacks [7, 13]. However, as a result of the power consumed by the BOP equipment, the alkaline electrolyzer has a higher specific energy consumption. If the power required for hydrogen compression is not considered, the specific energy consumption of the alkaline electrolyzer is 54.0 kWh/kg (4.9 kWh/Nm^3). Comparable values for the specific energy consumption of state-of-the-art alkaline electrolyzers have been reported by IRENA [15], which are typically between 47–66 kWh/kg. Likewise, the energy consumption of the alkaline electrolyzer per unit volume of hydrogen also agrees with the range of 4.5–7.0 kWh/Nm^3 reported for commercial alkaline electrolyzers in other previous publications [5, 13]. On the other hand, if hydrogen compression is considered for calculation of the specific energy consumption of the alkaline electrolyzer, the consumption of electrical energy per kilogram of compressed hydrogen at 200 bar increases slightly to 55.4 kWh/kg (5.0 kWh/Nm^3).

The hydrogen output from the alkaline water electrolyzer is at ambient temperature and slightly above ~15 bar, which means a density of only about 1.25 kg/m^3, a similar value to the density of ambient air. In order to enable the bulk gaseous storage of hydrogen in pressurized vessels with a reasonable energy density and relatively low power consumption, it has to be compressed in a multistage compression unit. The density of hydrogen after compression up to 200 bar is 15 kg/m^3, which gives an energy density of 1.8 GJ/m^3 based on the LHV. The energy requirement of hydrogen compression up to 200 bar in a single-stage compressor represents 5.56% of the energy content of hydrogen based on the LHV. By contrast, if a three-stage compressor with an equal pressure ratio between stages is used instead, the energy requirement of hydrogen compression

decreases significantly, amounting to 4.27% of the LHV of hydrogen.

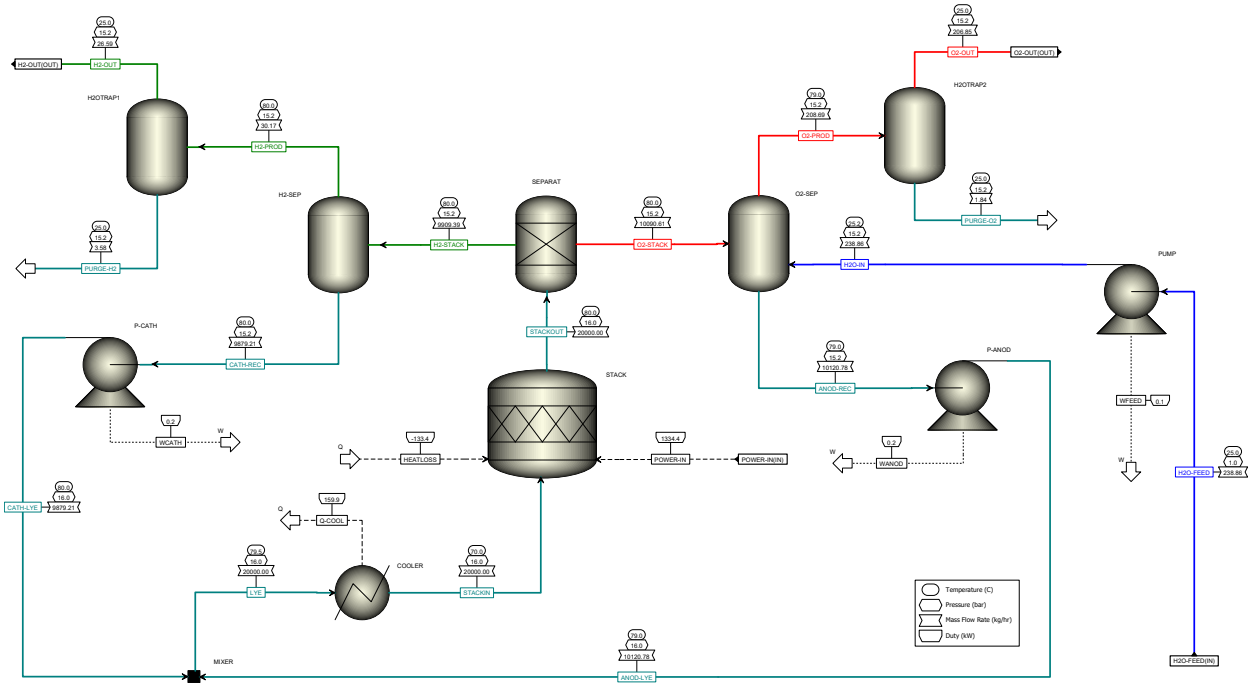

Figure 7: Process simulation flowsheet of the alkaline water electrolyzer in Aspen Plus. The size of the alkaline water electrolysis process is adjusted for a biomass consumption of 1 t/h in the hybrid IGCC-AWE plant.

The flow rate of oxygen obtained as a by-product in the alkaline water electrolysis process is enough to fire the downdraft gasifier in a self-sustaining process. As an example to prove this, let us suppose that the downdraft gasifier is sized for a biomass consumption of 1 t/h. In such case, the net AC power generation in the IGCC would be 1.45 MW, distributed as 1.14 MW in the topping power unit and 0.31 MW in the bottoming power unit. After subtraction of the power conversion losses in the rectifier, the power supply for hydrogen compression and the power consumption of the rest of the BOP equipment from the net AC power generation in the IGCC, the input DC power to the alkaline electrolysis stack is about 1.33 MW. The mass and energy flow balance of the alkaline water electrolysis process in closed circulation is displayed in Fig. 7. Temperatures, pressures and mass flow rates of the different streams are included, together with the heat losses and power consumption of the various unit operations. As mentioned above, the water electrolysis process is modeled within a hierarchy block, which has the demineralized

water supply and the DC power from the rectifier as inputs, while the outputs are the flow rates of hydrogen and oxygen at ambient temperature and process operating pressure. The alkaline electrolyzer is capable of continuously producing slightly more than 26 kg/h of hydrogen with a purity greater than 99.8%, which are eventually compressed to 200 bar in a three-stage compressor. The consumption of demineralized water in the alkaline electrolyzer to achieve that hydrogen production rate is approximately 239 kg/h. The heat loss in the stack is estimated as 10% of the total heat produced by the stack [10], namely about 133 kW. On the other hand, the flow rate of oxygen by-produced in the electrolyzer is just over 206 kg/h, with a purity greater than 99.9%. Thus, the flow rate of oxygen by-product from the electrolyzer is marginally higher than the flow rate of 204 kg/h required in the gasifier to ensure an oxygen concentration in the gasifying agent of at least 33% by volume. Furthermore, as previously reported, the air–fuel equivalence ratio (λ) must be higher or equal to 0.32 in order to reach a temperature above 1000 °C inside the gasifier, thereby minimizing tar formation. It is noteworthy that all these processes take place without the need for any external energy contribution beyond the biomass supply to the gasifier, and therefore, the hybrid IGCC-AWE plant can produce renewable hydrogen uninterruptedly in an off-grid mode.

3.5. Overall energy balance

In order to provide an overview of the energy flows and losses, Fig. 8 illustrates the overall energy balance of the hybrid IGCC-AWE plant in the form of a Sankey diagram. As evidenced in the energy balance, approximately 17.6% of the input chemical energy in the biomass feedstock to the downdraft gasifier eventually becomes renewable hydrogen in the alkaline water electrolyzer. The remaining 82.4% of the energy flow represents power consumption by the ancillary equipment, power conversion losses, heat losses and unrecovered heat. A significant share of the unrecoverable heat losses originates in the downdraft gasifier and producer gas conditioning unit, while the largest thermal losses as low-grade waste heat occur in the IGCC.

As defined by the cold gas efficiency, about 74.4% of the input chemical energy in the biomass feedstock remains in the conditioned producer gas. Heat transfer through the gasifier walls, dis-

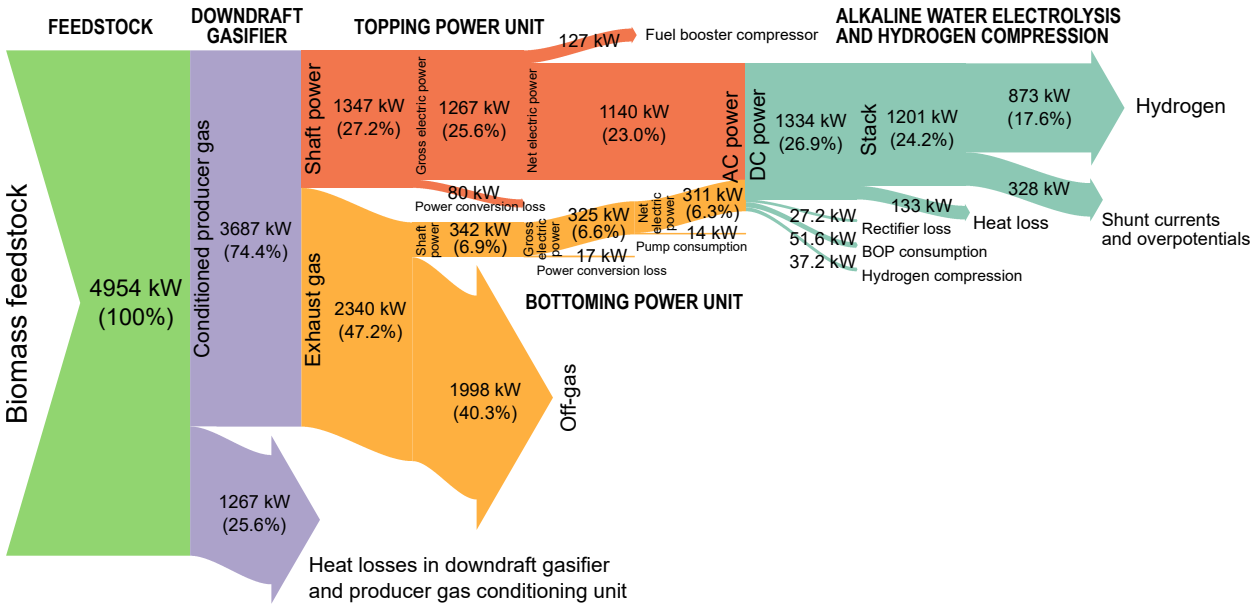

Figure 8: Energy flow diagram of the hybrid IGCC-AWE plant.

charge of hot solids (charcoal) and wet scrubbing of the producer gas are the main sources of energy loss during the gasification process and producer gas conditioning. An effective improvement measure to reduce the share of unrecoverable heat losses originating in the downdraft gasifier would be to incorporate a shell-and-tube heat exchanger just downstream of the hot producer gas discharge duct to preheat the inlet air to the gasifier. This improvement measure would allow to reduce the value of λ required to reach a sufficiently high temperature inside the gasifier to minimize tar formation, thereby increasing the cold gas efficiency. However, this waste heat recovery configuration is not widely used in commercial biomass gasification plants, because the heat exchanger requires costly materials for high-temperature operation and also introduces severe maintenance issues due to the presence of tar, ash and soot in the hot producer gas. These impurities can condense, foul and form unwanted material deposits on heat transfer surfaces, which significantly reduce the heat transfer efficiency and could even block the shell and tubes. Therefore, the option of including a heat exchanger prior to the producer gas conditioning unit is not considered in this work.

As mentioned above, the conditioned producer gas is eventually used as fuel for the topping

power unit, which consists of a recuperative gas turbine with a net electrical efficiency of 30.9%. Consequently, the net power from the topping power unit corresponds to approximately 23.0% of the input energy flow. The hot exhaust gas is discharged from the recuperator of the gas turbine at a temperature of around 290 °C, which represents about 47.2% of the input energy flow. The exhaust gas stream is used to drive a bottoming power unit consisting of a regenerative organic Rankine cycle, with a net electrical efficiency of 13.1%, which allows to recover about 6.3% of the input energy flow. Accordingly, the net electrical efficiency of the combined cycle is 39.4% based on the LHV of the conditioned producer gas. The off-gas from the evaporator of the organic Rankine cycle is at a temperature close to 100 °C, which constitutes about 40.3% of the input energy flow. This low-grade waste heat could be partially recovered for combined heat and power (CHP) in the event that there is a thermal demand to be satisfied, which is usual in some industries, thereby significantly increasing the overall efficiency of the hybrid IGCC-AWE plant. On the other hand, the net AC power generation in the IGCC represents 29.3% of the input energy flow.

The net AC power from the IGCC is used to power the alkaline water electrolyzer, including all the utilities that are part of the BOP equipment and the multistage hydrogen compressor. The power consumption of all the ancillary equipment of the alkaline water electrolyzer is estimated at 8% of the gross electric power generation in the IGCC. After subtraction of the power conversion losses in the rectifier together with the power consumed by the BOP equipment and the hydrogen compressor from the AC power generated in the IGCC, the net DC power that is supplied to the alkaline water electrolysis stack contributes to 26.9% of the input energy flow. The heat losses, faradaic losses, shunt currents and overpotentials that occur in the alkaline water electrolysis stack cause the efficiency of the stack (η_{stack}) to be 65.4%, and therefore, the hydrogen obtained as a final product eventually contains about 17.6% of the input energy flow. The yield of compressed hydrogen at 200 bar is approximately 26 g/kg biomass feedstock. Comparable values for the hydrogen yields of other process options (thermochemical, biological and electrochemical technologies) to produce hydrogen from biomass have been reported in the literature. A SWOT (strengths, weak-

nesses, opportunities and threats) analysis of these process options can be consulted in a recent review article [2], which includes the hydrogen yields (expressed in g/kg biomass feedstock) of each technology, together with their main advantages and drawbacks. Even though the global efficiency of the hybrid IGCC-AWE plant ($\eta_{\text{IGCC-AWE}}$) may appear rather modest, it is noteworthy that it includes hydrogen compression up to 200 bar and no external power consumption is required after commissioning. Moreover, the alkaline water electrolysis process can deliver a high-purity hydrogen gas (>99.8%) [5], and thus, downstream purification operations are not required. Another important advantage worth mentioning is that all the processes and equipment are at a high level of technological maturity and can be modular. However, the integration of these processes and equipment to achieve optimal performance, as well as the economic competitiveness of the whole plant may be challenging, which would require a subsequent detailed techno-economic assessment and sensitivity analysis.

4. Conclusions

This research work is intended to serve as a proof of concept for continuous decentralized high-purity green hydrogen production from woody biomass through hybridization of an integrated gasification combined cycle (IGCC) and alkaline water electrolysis (AWE). The IGCC consists of a downdraft fixed bed gasifier, a recuperative gas turbine as topping unit and a subcritical regenerative organic Rankine cycle as bottoming unit, which allows a combined power generation efficiency close to 30% (based on the LHV of the biomass feedstock). On the other hand, the efficiency of the alkaline electrolyzer, including the power consumption by the ancillary equipment and hydrogen compression to 200 bar, is just over 60% (based on the LHV of hydrogen). Accordingly, the hydrogen production efficiency of the hybrid IGCC-AWE is slightly below 18%, which is a reasonable value, since a solid biomass feedstock with a relatively low calorific value is being used to drive the entire system.

Despite its modest efficiency, the hybrid IGCC-AWE system presents several major advantages

for decentralized high-purity green hydrogen production, such as the high level of technological maturity of the equipment (all the units are at TRL 9 and commercially available), which can be modular, and the very high capacity factor of the IGCC, which enables operation of the electrolyzer at full load with a prolonged lifetime, thereby maximizing the hydrogen production over the electrolyzer's entire lifetime as a result of its very high utilization factor. Moreover, since the oxygen produced during alkaline water electrolysis is usually released into the atmosphere as a worthless by-product, hybridization of this technology with biomass gasification represents a very promising alternative to substantially improve the performance of the combined system.

The hydrogen production approach explored in this work does not allow to fire the downdraft gasifier with pure oxygen because the flow rate of oxygen by-product from the alkaline electrolyzer placed downstream is limited. However, oxygen-enriched air with a concentration of oxygen up to 32% can be used as gasifying agent instead of ambient air, thereby leading to an upgraded producer gas with a substantially lower nitrogen content, and hence, a higher calorific value. The upgraded producer gas can then be used to effectively improve the performance of the IGCC. However, further research and development is needed to address challenges such as the economic competitiveness of this hydrogen production approach, since the capital investment of the required equipment is expected to be considerably high.

Regardless of the renewable power generation technology used to power the electrolyzers, the unprecedented momentum that the electrolytic production of green hydrogen is experiencing may act as a driver for the development of oxy-fired biomass gasification systems, since there will likely be a substantial excess of oxygen as a by-product. However, in a scenario dominated by fluctuating renewable electricity generation technologies, the surplus oxygen from water electrolysis could be better used to further increase hydrogen production through oxy-fired biomass gasification and several subsequent stages of hydrogen concentration, separation and purification, which is where the authors see the greatest potential from an economic standpoint once the required technology has reached a state of maturity and becomes commercially available. This approach is also not

without drawbacks, as it would require a stable supply of renewable electricity previously stored in batteries or similar energy storage devices to ensure that the electrolyzers are operating under nominal load, or alternatively, storage in pressurized vessels of the unstable and unpredictable oxygen supply from the electrolyzers operating under variable load to avoid the challenging dynamic operation of the oxy-fired biomass gasification process.

Nomenclature

Symbols

A	Area [m^2]
c_p	Mass heat capacity at constant pressure [$kJ \cdot kg^{-1} \cdot K^{-1}$]
F	Faraday constant [$A \cdot s \cdot mol^{-1}$]
G	Gibbs free energy [kJ]
h	Specific enthalpy [$kJ \cdot kg^{-1}$]
H	Enthalpy [kJ]
i	Current density [$A \cdot m^{-2}$]
$\dot{m}$	Mass flow rate [$kg \cdot s^{-1}$]
M	Molar mass [$kg \cdot kmol^{-1}$]
$\dot{n}$	Mole flow rate [$kmol \cdot s^{-1}$]
N	Number of cells
p	Pressure [bar]
P	Power [kW]

S Entropy [kJ·K^{-1}]

T Temperature [K]

V Voltage [V]

x Mass fraction

y Mole fraction

z Number of electrons

Greek letters

ε Heat transfer effectiveness

η Efficiency

ϕ Fuel–oxidizer equivalence ratio

λ Oxidizer–fuel equivalence ratio

Π Pressure ratio

Subscripts

a Ambient

bottom Bottoming power cycle

cell Electrolysis cell

cg Conditioned producer gas

comp Compressor

cond Condenser

conv Power conversion

eg Exhaust gas

em Electromechanical

evap Evaporator

exp Expander

f Feedstock or fuel

gen Generator

gturb Gas turbine

i Isentropic

m Mechanical

og Off-gas

rev Reversible

tn Thermoneutral

top Topping power cycle

wf Working fluid

Abbreviations

AC Alternating current

AWE Alkaline water electrolysis (including hydrogen compression)

BOP Balance of plant

CHP Combined heat and power

DC Direct current

GWP Global warming potential

HHV Higher heating value [MJ·kg^{-1}]

HRSG Heat recovery steam generator

IGCC Integrated gasification combined cycle

LHV Lower heating value [MJ·kg^{-1}]

ORC Organic Rankine cycle

PSA Pressure swing adsorption

SATP Standard ambient temperature and pressure (25 °C, 1 bar)

SNG Synthetic natural gas

TIT Turbine inlet temperature

TRL Technology readiness level

CRediT authorship contribution statement

R. Aguado: Conceptualization, Data curation, Formal analysis, Investigation, Methodology, Validation, Visualization, Writing - Original Draft, Writing - Review & Editing. **A. Baccioli:** Investigation, Methodology, Resources, Supervision, Validation. **A. Liponi:** Formal analysis, Investigation, Resources, Validation, Writing - Review & Editing. **D. Vera:** Conceptualization, Funding acquisition, Investigation, Project administration, Supervision, Validation.

Declaration of competing interest

The authors declare no known personal or financial competing interest.

Funding

This research work was supported by the project entitled "Renewable energies for Africa: Effective valorisation of agri-food wastes (REFFECT AFRICA)", which has received funding from the *European Union's Horizon 2020 Research and Innovation Programme* under the following Grant Agreement ID number: 101036900.

Roque Aguado gratefully acknowledges financial support from *Ministerio de Universidades* under the FPU Programme (Ref. FPU19/00930). Additionally, he thanks *Universidad de Jaén* for funding his international research stay at *Università di Pisa* under *Plan Operativo de Apoyo a la Investigación 2021–2022*.

References

[1] M. Buffi, M. Prussi, N. Scarlat, Energy and environmental assessment of hydrogen from biomass sources: Challenges and perspectives, Biomass Bioenerg. 165 (2022) 106556. doi:10.1016/j.biombioe.2022.106556.

[2] T. Lepage, M. Kammoun, Q. Schmetz, A. Richel, Biomass-to-hydrogen: A review of main routes production, processes evaluation and techno-economical assessment, Biomass Bioenerg. 144 (2021) 105920. doi:10.1016/j.biombioe.2020.105920.

[3] T. K. Patra, S. Mukherjee, P. N. Sheth, Process simulation of hydrogen rich gas production from producer gas using HTS catalysis, Energy 173 (2019) 1130–1140. doi:10.1016/j.energy.2019.02.136.

[4] International Renewable Energy Agency (IRENA), Hydrogen: A renewable energy perspective, https://www.irena.org/-/media/Files/IRENA/Agency/Publication/2019/Sep/IRENA_Hydrogen_2019.pdf, Accessed: 2022-10-18 (2019).

[5] I. Dincer, C. Acar, Review and evaluation of hydrogen production methods for better sustainability, Int. J. Hydrog. Energy 40 (34) (2015) 11094–11111. doi:10.1016/j.ijhydene.2014.12.035.

[6] P. Nikolaidis, A. Poullikkas, A comparative overview of hydrogen production processes, Renew. Sust. Energ. Rev. 67 (2017) 597–611. doi:10.1016/j.rser.2016.09.044.

[7] M. David, C. Ocampo-Martínez, R. Sánchez-Peña, Advances in alkaline water electrolyzers: A review, J. Energy Storage 23 (2019) 392–403. doi:10.1016/j.est.2019.03.001.

[8] J. Brauns, T. Turek, Alkaline water electrolysis powered by renewable energy: A review, Processes 8 (2) (2020). doi:10.3390/pr8020248.

[9] A. Baccioli, E. Bargiacchi, S. Barsali, A. Ciambellotti, D. Fioriti, R. Giglioli, G. Pasini, Cost effective power-to-X plant using carbon dioxide from a geothermal plant to increase renewable energy penetration, Energy Convers. Manag. 226 (2020) 113494. doi:10.1016/j.enconman.2020.113494.

[10] M. Sánchez, E. Amores, D. Abad, L. Rodríguez, C. Clemente-Jul, Aspen Plus model of an alkaline electrolysis system for hydrogen production, Int. J. Hydrog. Energy 45 (7) (2020) 3916–3929. doi:10.1016/j.ijhydene.2019.12.027.

[11] A. Liponi, A. Baccioli, L. Ferrari, U. Desideri, Techno-economic analysis of hydrogen production from PV plants, E3S Web Conf. 334 (2022) 01001. doi:10.1051/e3sconf/202233401001.

[12] H. Nami, O. B. Rizvandi, C. Chatzichristodoulou, P. V. Hendriksen, H. L. Frandsen, Techno-economic analysis of current and emerging electrolysis technologies for green hydrogen production, Energy Convers. Manag. 269 (2022) 116162. doi:10.1016/j.enconman.2022.116162.

[13] A. Buttler, H. Spliethoff, Current status of water electrolysis for energy storage, grid balancing and sector coupling via power-to-gas and power-to-liquids: A review, Renew. Sust. Energ. Rev. 82 (2018) 2440–2454. doi:10.1016/j.rser.2017.09.003.

[14] Ø. Ulleberg, Modeling of advanced alkaline electrolyzers: a system simulation approach, Int. J. Hydrog. Energy 28 (1) (2003) 21–33. doi:10.1016/S0360-3199(02)00033-2.

[15] International Renewable Energy Agency (IRENA), Green Hydrogen Cost Reduction: Scaling up Electrolysers to Meet the 1.5 °C Climate Goal, https://www.irena.org/-/media/Files/IRENA/Agency/Publication/2020/Dec/IRENA_Green_hydrogen_cost_2020.pdf?rev=4ce868aa69b54674a789f990e85a3f00, Accessed: 2022-10-18 (2020).

[16] M. Sánchez, E. Amores, L. Rodríguez, C. Clemente-Jul, Semi-empirical model and experimental validation for the performance evaluation of a 15 kW alkaline water electrolyzer, Int. J. Hydrog. Energy 43 (45) (2018) 20332–20345. doi:10.1016/j.ijhydene.2018.09.029.

[17] P. Diéguez, A. Ursúa, P. Sanchis, C. Sopena, E. Guelbenzu, L. Gandía, Thermal performance of a commercial alkaline water electrolyzer: Experimental study and mathematical modeling, Int. J. Hydrog. Energy 33 (24) (2008) 7338–7354. doi:10.1016/j.ijhydene.2008.09.051.

[18] G. Matute, J. Yusta, L. Correas, Techno-economic modelling of water electrolysers in the range of several MW

to provide grid services while generating hydrogen for different applications: A case study in Spain applied to mobility with FCEVs, Int. J. Hydrog. Energy 44 (33) (2019) 17431–17442. doi:10.1016/j.ijhydene.2019.05.092.

[19] E. Biagini, L. Masoni, L. Tognotti, Comparative study of thermochemical processes for hydrogen production from biomass fuels, Bioresour. Technol. 101 (16) (2010) 6381–6388. doi:10.1016/j.biortech.2010.03.052.

[20] L. Menin, S. Vakalis, V. Benedetti, F. Patuzzi, M. Baratieri, Techno-economic assessment of an integrated biomass gasification, electrolysis, and syngas biomethanation process, Biomass Conv. Bioref. 11 (2) (2021) 445–459. doi:10.1007/s13399-020-00654-9.

[21] M. Binder, M. Kraussler, M. Kuba, M. Luisser, Hydrogen from biomass gasification, IEA Bioenergy, https://www.ieabioenergy.com/wp-content/uploads/2019/01/Wasserstoffstudie_IEA-final.pdf, Accessed: 2022-10-18 (2018).

[22] A. Liponi, G. F. Frate, A. Baccioli, L. Ferrari, U. Desideri, Impact of wind speed distribution and management strategy on hydrogen production from wind energy, Energy 256 (2022) 124636. doi:10.1016/j.energy.2022.124636.

[23] T. Kato, M. Kubota, N. Kobayashi, Y. Suzuoki, Effective utilization of by-product oxygen from electrolysis hydrogen production, Energy 30 (14) (2005) 2580–2595. doi:10.1016/j.energy.2004.07.004.

[24] M. Bailera, P. Lisbona, L. M. Romeo, Power to gas-oxyfuel boiler hybrid systems, Int. J. Hydrog. Energy 40 (32) (2015) 10168–10175. doi:10.1016/j.ijhydene.2015.06.074.

[25] M. Bailera, S. Espatolero, P. Lisbona, L. M. Romeo, Power to gas-electrochemical industry hybrid systems: A case study, Appl. Energy 202 (2017) 435–446. doi:10.1016/j.apenergy.2017.05.177.

[26] S. Frigo, G. Spazzafumo, Comparison of different system layouts to generate a substitute of natural gas from biomass and electrolytic hydrogen, Int. J. Hydrog. Energy 45 (49) (2020) 26166–26178. doi:10.1016/j.ijhydene.2020.03.205.

[27] S. Ali, K. Sørensen, M. P. Nielsen, Modeling a novel combined solid oxide electrolysis cell (SOEC) - Biomass gasification renewable methanol production system, Renew. Energy 154 (2020) 1025–1034. doi:10.1016/j.renene.2019.12.108.

[28] H. Zhang, L. Wang, M. Pérez-Fortes, J. Van herle, F. Maréchal, U. Desideri, Techno-economic optimization of biomass-to-methanol with solid-oxide electrolyzer, Appl. Energy 258 (2020) 114071. doi:10.1016/j.apenergy.2019.114071.

[29] E. Giglio, G. Vitale, A. Lanzini, M. Santarelli, Integration between biomass gasification and high-temperature

electrolysis for synthetic methane production, Biomass Bioenerg. 148 (2021) 106017. doi:10.1016/j.biombioe.2021.106017.

[30] P. Basu, Biomass Gasification, Pyrolysis and Torrefaction, 3rd Edition, Academic Press, 2018. doi:10.1016/C2016-0-04056-1.

[31] A. Bridgwater, The technical and economic feasibility of biomass gasification for power generation, Fuel 74 (5) (1995) 631–653. doi:10.1016/0016-2361(95)00001-L.

[32] P. Sittisun, N. Tippayawong, S. Pang, Biomass gasification in a fixed bed downdraft reactor with oxygen enriched air: a modified equilibrium modeling study, Energy Procedia 160 (2019) 317–323. doi:10.1016/j.egypro.2019.02.163.

[33] A. Bhattacharya, A. Bhattacharya, A. Datta, Modeling of hydrogen production process from biomass using oxygen blown gasification, Int. J. Hydrog. Energy 37 (24) (2012) 18782–18790. doi:10.1016/j.ijhydene.2012.09.131.

[34] J. Sánchez, M. Barreiro, M. Maroño, Hydrogen enrichment and separation from synthesis gas by the use of a membrane reactor, Biomass Bioenerg. 35 (2011) S132–S144. doi:10.1016/j.biombioe.2011.03.037.

[35] J. Yao, M. Kraussler, F. Benedikt, H. Hofbauer, Techno-economic assessment of hydrogen production based on dual fluidized bed biomass steam gasification, biogas steam reforming, and alkaline water electrolysis processes, Energy Convers. Manag. 145 (2017) 278–292. doi:10.1016/j.enconman.2017.04.084.

[36] P. Hulteberg, H. Karlsson, A study of combined biomass gasification and electrolysis for hydrogen production, Int. J. Hydrog. Energy 34 (2) (2009) 772–782. doi:10.1016/j.ijhydene.2008.10.073.

[37] J. Kalina, Techno-economic assessment of small-scale integrated biomass gasification dual fuel combined cycle power plant, Energy 141 (2017) 2499–2507. doi:10.1016/j.energy.2017.05.009.

[38] M. Hosseinpour, H. A. Ozgoli, S. A. Hajiseyed Mirzahosseini, A. H. Hemmasi, R. Mehdipour, Evaluation of performance improvement of the combined biomass gasifier power cycle using low-temperature bottoming cycles: Organic Rankine cycle, Kalina and Goswami, Environ. Prog. Sustain. Energy 41 (5) (2022) e13855. doi:10.1002/ep.13855.

[39] M. Niu, J. Xie, S. Liang, L. Liu, L. Wang, Y. Peng, Simulation of a new biomass integrated gasification combined cycle (BIGCC) power generation system using Aspen Plus: Performance analysis and energetic assessment, Int. J. Hydrog. Energy 46 (43) (2021) 22356–22367. doi:10.1016/j.ijhydene.2021.04.076.

[40] G. Zang, J. Zhang, J. Jia, E. S. Lora, A. Ratner, Life cycle assessment of power-generation systems based on biomass integrated gasification combined cycles, Renew. Energy 149 (2020) 336–346. doi:10.1016/j.renene.2019.12.013.

[41] A. Gagliano, F. Nocera, M. Bruno, G. Cardillo, Development of an Equilibrium-based Model of Gasification of Biomass by Aspen Plus, Energy Procedia 111 (2017) 1010–1019. doi:10.1016/j.egypro.2017.03.264.

[42] R. Tavares, E. Monteiro, F. Tabet, A. Rouboa, Numerical investigation of optimum operating conditions for syngas and hydrogen production from biomass gasification using Aspen Plus, Renew. Energy 146 (2020) 1309–1314. doi:10.1016/j.renene.2019.07.051.

[43] Y. Cao, Q. Wang, J. Du, J. Chen, Oxygen-enriched air gasification of biomass materials for high-quality syngas production, Energy Convers. Manag. 199 (2019) 111628. doi:10.1016/j.enconman.2019.05.054.

[44] N. Henao, E. Lora, D. Maya, O. Venturini, E. Franco, Technical feasibility study of 200 kW gas microturbine coupled to a dual fluidized bed gasifier, Biomass Bioenerg. 130 (2019) 105369. doi:10.1016/j.biombioe.2019.105369.

[45] W. Liu, Y. Tian, H. Yan, X. Zhou, Y. Tan, Y. Yang, Z. Li, L. Yuan, Gasification of biomass using oxygen-enriched air as gasification agent: a simulation study, Biomass Conv. Bioref. (2021). doi:10.1007/s13399-021-02035-2.

[46] Aspen Technology, Inc. (AspenTech), Physical Property Methods and Models 11.1 (2001).

[47] M. Formica, S. Frigo, R. Gabbrielli, Development of a new steady state zero-dimensional simulation model for woody biomass gasification in a full scale plant, Energy Convers. Manag. 120 (2016) 358–369. doi:10.1016/j.enconman.2016.05.009.

[48] E. Shayan, V. Zare, I. Mirzaee, Hydrogen production from biomass gasification: a theoretical comparison of using different gasification agents, Energy Convers. Manag. 159 (2018) 30–41. doi:10.1016/j.enconman.2017.12.096.

[49] H. Wiinikka, J. Wennebro, M. Gullberg, E. Pettersson, F. Weiland, Pure oxygen fixed-bed gasification of wood under high temperature (>1000°C) freeboard conditions, Appl. Energy 191 (2017) 153–162. doi:10.1016/j.apenergy.2017.01.054.

[50] L. Liu, Y. Huang, J. Cao, C. Liu, L. Dong, L. Xu, J. Zha, Experimental study of biomass gasification with oxygen-enriched air in fluidized bed gasifier, Sci. Total Environ. 626 (2018) 423–433. doi:10.1016/j.scitotenv.2018.01.016.

[51] D. Baruah, D. Baruah, Modeling of biomass gasification: A review, Renew. Sust. Energ. Rev. 39 (2014) 806–815. doi:10.1016/j.rser.2014.07.129.

[52] C. R. Altafini, P. R. Wander, R. M. Barreto, Prediction of the working parameters of a wood waste gasifier through an equilibrium model, Energy Convers. Manag. 44 (17) (2003) 2763–2777. doi:10.1016/S0196-8904(03)00025-6.

[53] S. Jarungthammachote, A. Dutta, Equilibrium modeling of gasification: Gibbs free energy minimization approach and its application to spouted bed and spout-fluid bed gasifiers, Energy Convers. Manag. 49 (6) (2008) 1345–1356. doi:10.1016/j.enconman.2008.01.006.

[54] L. Fryda, K. Panopoulos, E. Kakaras, Integrated CHP with autothermal biomass gasification and SOFC–MGT, Energy Convers. Manag. 49 (2) (2008) 281–290. doi:10.1016/j.enconman.2007.06.013.

[55] D. Vera, F. Jurado, K. D. Panopoulos, P. Grammelis, Modelling of biomass gasifier and microturbine for the olive oil industry, Int. J. Energy Res. 36 (3) (2012) 355–367. doi:10.1002/er.1802.

[56] D. Vera, F. Jurado, J. Carpio, S. Kamel, Biomass gasification coupled to an EFGT-ORC combined system to maximize the electrical energy generation: A case applied to the olive oil industry, Energy 144 (2018) 41–53. doi:10.1016/j.energy.2017.11.152.

[57] Ö. Ç. Mutlu, T. Zeng, Challenges and opportunities of modeling biomass gasification in Aspen Plus: A review, Chem. Eng. Technol. 43 (9) (2020) 1674–1689. doi:10.1002/ceat.202000068.

[58] A. Abuadala, I. Dincer, G. Naterer, Exergy analysis of hydrogen production from biomass gasification, Int. J. Hydrog. Energy 35 (10) (2010) 4981–4990. doi:10.1016/j.ijhydene.2009.08.025.

[59] W. Lan, G. Chen, X. Zhu, X. Wang, C. Liu, B. Xu, Biomass gasification-gas turbine combustion for power generation system model based on ASPEN PLUS, Sci. Total Environ. 628-629 (2018) 1278–1286. doi:10.1016/j.scitotenv.2018.02.159.

[60] G. Zang, S. Tejasvi, A. Ratner, E. S. Lora, A comparative study of biomass integrated gasification combined cycle power systems: Performance analysis, Bioresour. Technol. 255 (2018) 246–256. doi:10.1016/j.biortech.2018.01.093.

[61] M. L. Valderrama Ríos, A. Martínez González, E. E. Silva Lora, O. A. Almazán del Olmo, Reduction of tar generated during biomass gasification: A review, Biomass Bioenerg. 108 (2018) 345–370. doi:10.1016/j.biombioe.2017.12.002.

[62] P. Pilavachi, Mini- and micro-gas turbines for combined heat and power, Appl. Therm. Eng. 22 (18) (2002) 2003–2014. doi:10.1016/S1359-4311(02)00132-1.

[63] M. C. Lee, J. Yoon, S. Joo, Y. Yoon, Gas turbine combustion characteristics of H_2/CO synthetic gas for coal integrated gasification combined cycle applications, Int. J. Hydrog. Energy 40 (34) (2015) 11032–11045. doi:10.1016/j.ijhydene.2015.06.086.

[64] Fundamental impact of firing syngas in gas turbines, Vol. Volume 3: Turbo Expo 2007. doi:10.1115/GT2007-27385.

[65] C. Ghenai, Combustion of syngas fuel in gas turbine can combustor, Adv. Mech. Eng. 2 (2010) 342357. doi:

10.1155/2010/342357.

[66] Numerical analysis of a microturbine combustion chamber modified for biomass derived syngas, Vol. Volume 2: Combustion, Fuels and Emissions, Parts A and B of Turbo Expo: Power for Land, Sea, and Air. doi:10.1115/GT2011-45551.

[67] C. Mărculescu, V. E. Cenuşă, F. N. Alexe, Analysis on using biomass lean syngas in micro gas turbines, IOP Conference Series: Earth and Environmental Science 40 (1) (2016) 012036. doi:10.1088/1755-1315/40/1/012036.

[68] W. de Paepe, S. Abraham, P. Tsirikoglou, F. Contino, A. Parente, G. Ghorbaniasl, Operational optimization of a typical micro gas turbine, Energy Procedia 142 (2017) 1653–1660. doi:10.1016/j.egypro.2017.12.545.

[69] W. de Paepe, D. Coppitters, S. Abraham, P. Tsirikoglou, G. Ghorbaniasl, F. Contino, Robust operational optimization of a typical micro gas turbine, Energy Procedia 158 (2019) 5795–5803. doi:10.1016/j.egypro.2019.01.549.

[70] R. K. Shah, Compact heat exchangers for microturbines, in: Micro Gas Turbines, Educational Notes RTO-EN-AVT-131, 2005, pp. 1–18, https://www.sto.nato.int/publications/STO%20Educational%20Notes/RTO-EN-AVT-131/EN-AVT-131-02.pdf.

[71] Materials selection for high temperature (750-1000°C) metallic recuperators for improved efficiency microturbines, Vol. Volume 1: Aircraft Engine; Marine; Turbomachinery; Microturbines and Small Turbomachinery of Turbo Expo: Power for Land, Sea, and Air. doi:10.1115/2001-GT-0445.

[72] C. Carcasci, L. Winchler, Thermodynamic analysis of an organic Rankine cycle for waste heat recovery from an aeroderivative intercooled gas turbine, Energy Procedia 101 (2016) 862–869. doi:10.1016/j.egypro.2016.11.109.

[73] R. Chacartegui, D. Sánchez, J. Muñoz, T. Sánchez, Alternative ORC bottoming cycles for combined cycle power plants, Appl. Energy 86 (10) (2009) 2162–2170. doi:10.1016/j.apenergy.2009.02.016.

[74] S. Quoilin, M. V. D. Broek, S. Declaye, P. Dewallef, V. Lemort, Techno-economic survey of organic Rankine cycle (ORC) systems, Renew. Sust. Energ. Rev. 22 (2013) 168–186. doi:10.1016/j.rser.2013.01.028.

[75] A. Ghilardi, G. F. Frate, A. Baccioli, D. Ulivieri, L. Ferrari, U. Desideri, L. Cosi, S. Amidei, V. Michelassi, Techno-economic comparison of several technologies for waste heat recovery of gas turbine exhausts, J. Eng. Gas Turbines Power (2022). doi:10.1115/1.4055872.

[76] A. Auld, A. Berson, S. Hogg, Organic Rankine cycles in waste heat recovery: A comparative study, Int. J. Low-Carbon Technol. 8 (2013) i9–i18. doi:10.1093/ijlct/ctt033.

[77] D. Dragomir-Stanciu, S. M. Saghebian, A. Kurchania, The influence of condensing temperature on the efficiency

of solar power systems with ORC, Procedia Manufacturing 46 (2020) 359–363. doi:10.1016/j.promfg.2020.03.052.

[78] U. Drescher, D. Brüggemann, Fluid selection for the Organic Rankine Cycle (ORC) in biomass power and heat plants, Appl. Therm. Eng. 27 (1) (2007) 223–228. doi:10.1016/j.applthermaleng.2006.04.024.

[79] H. Herath, M. Wijewardane, R. Ranasinghe, J. Jayasekera, Working fluid selection of Organic Rankine Cycles, Energy Reports 6 (2020) 680–686. doi:10.1016/j.egyr.2020.11.150.

[80] P. J. Mago, L. M. Chamra, K. Srinivasan, C. Somayaji, An examination of regenerative organic Rankine cycles using dry fluids, Appl. Therm. Eng. 28 (8) (2008) 998–1007. doi:10.1016/j.applthermaleng.2007.06.025.

[81] J. Bao, L. Zhao, A review of working fluid and expander selections for organic Rankine cycle, Renew. Sust. Energ. Rev. 24 (2013) 325–342. doi:10.1016/j.rser.2013.03.040.

[82] K. Rahbar, S. Mahmoud, R. K. Al-Dadah, N. Moazami, S. A. Mirhadizadeh, Review of organic Rankine cycle for small-scale applications, Energy Convers. Manag. 134 (2017) 135–155. doi:10.1016/j.enconman.2016.12.023.

[83] E. Macchi, Theoretical basis of the Organic Rankine Cycle, in: E. Macchi, M. Astolfi (Eds.), Organic Rankine Cycle (ORC) Power Systems, Woodhead Publishing, 2017, pp. 3–24. doi:10.1016/B978-0-08-100510-1.00001-6.

[84] E. Lemmon, M. Huber, M. McLinden, NIST Standard Reference Database 23: Reference Fluid Thermodynamic and Transport Properties-REFPROP, Version 8.0 (2007).

[85] C. Invernizzi, D. Bonalumi, Thermal stability of organic fluids for Organic Rankine Cycle systems, in: E. Macchi, M. Astolfi (Eds.), Organic Rankine Cycle (ORC) Power Systems, Woodhead Publishing, 2017, pp. 121–151. doi:10.1016/B978-0-08-100510-1.00005-3.

[86] A. Baccioli, M. Antonelli, U. Desideri, Technical and economic analysis of organic flash regenerative cycles (OFRCs) for low temperature waste heat recovery, Appl. Energy 199 (2017) 69–87. doi:10.1016/j.apenergy.2017.04.058.

[87] A. Baccioli, M. Antonelli, Organic Flash Cycles: Off-design behavior and control strategies of two different cycle architectures for Waste Heat Recovery applications, Energy Convers. Manag. 157 (2018) 176–185. doi:10.1016/j.enconman.2017.12.004.

[88] A. Mohammadi, A. Kasaeian, F. Pourfayaz, M. H. Ahmadi, Thermodynamic analysis of a combined gas turbine, ORC cycle and absorption refrigeration for a CCHP system, Appl. Therm. Eng. 111 (2017) 397–406. doi:10.1016/j.applthermaleng.2016.09.098.

[89] G. Sakas, A. Ibáñez-Rioja, V. Ruuskanen, A. Kosonen, J. Ahola, O. Bergmann, Dynamic energy and mass balance model for an industrial alkaline water electrolyzer plant process, Int. J. Hydrog. Energy 47 (7) (2022) 4328–4345. doi:10.1016/j.ijhydene.2021.11.126.

[90] S. Grigoriev, V. Fateev, D. Bessarabov, P. Millet, Current status, research trends, and challenges in water electrolysis science and technology, Int. J. Hydrog. Energy 45 (49) (2020) 26036–26058. doi:10.1016/j.ijhydene.2020.03.109.

[91] J. Zheng, X. Liu, P. Xu, P. Liu, Y. Zhao, J. Yang, Development of high pressure gaseous hydrogen storage technologies, Int. J. Hydrog. Energy 37 (1) (2012) 1048–1057. doi:10.1016/j.ijhydene.2011.02.125.

[92] D. Grouset, C. Ridart, Chapter 6 - lowering energy spending together with compression, storage, and transportation costs for hydrogen distribution in the early market, in: C. Azzaro-Pantel (Ed.), Hydrogen Supply Chains, Academic Press, 2018, pp. 207–270. doi:10.1016/B978-0-12-811197-0.00006-3.

[93] M.-R. Tahan, Recent advances in hydrogen compressors for use in large-scale renewable energy integration, Int. J. Hydrog. Energy 47 (83) (2022) 35275–35292. doi:10.1016/j.ijhydene.2022.08.128.

[94] G. Cheng, P.-W. He, B. Xiao, Z.-Q. Hu, S.-M. Liu, L.-G. Zhang, L. Cai, Gasification of biomass micron fuel with oxygen-enriched air: Thermogravimetric analysis and gasification in a cyclone furnace, Energy 43 (1) (2012) 329–333. doi:10.1016/j.energy.2012.04.022.

[95] J. Yang, Z. Sun, B. Yu, J. Chen, Experimental comparison and optimization guidance of R1233zd(E) as a drop-in replacement to R245fa for organic Rankine cycle application, Appl. Therm. Eng. 141 (2018) 10–19. doi:10.1016/j.applthermaleng.2018.05.105.